LSC

Laboratorio Subterráneo de Canfranc

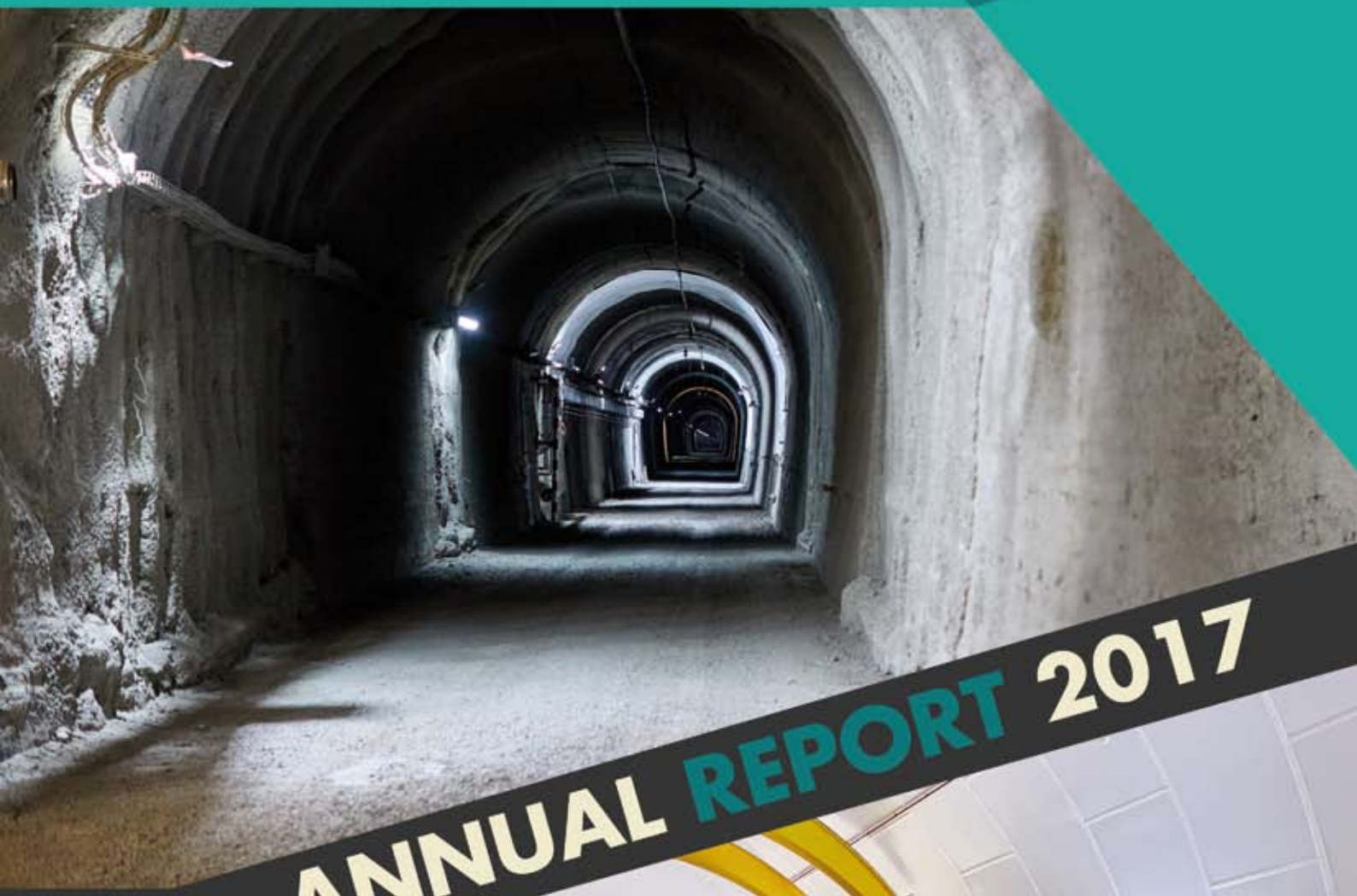

ANNUAL REPORT 2017

EDITING

Aldo Ianni

Yolanda Labarta

COVER PHOTOS:

Railway Tunnel and Hall A
(Photos by J. Larrea)

Thanks to all who helped towards the making of this editorial project

LSC
Laboratorio Subterráneo de Canfranc

Paseo de los Ayerbe, s/n

Canfranc Estación

22880 (Huesca)

ESPAÑA

http://www.lsc-canfranc.es

Tel: +34 974 373 474

CONTENTS

DIRECTOR'S STATEMENT

The LSC (Laboratorio Subterráneo de Canfranc) is the second largest deep underground scientific laboratory in Europe. It is run by a Consortium between the Spanish "Ministerio de Economía Industria y Competitividad", the "Gobierno de Aragón" and the University of Zaragoza. LSC belongs to the Spanish network of ICTS "Infraestructura Científica Tecnológica Singular" (Unique Scientific and Technological Facilities).

The LSC offers to researchers from all over the world the opportunity to carry out world-class science on fundamental physics, astrophysics, geophysics, biology and, environmental science in a location of unique characteristics. In fact, at the LSC the underground facilities, shielded from the natural cosmic rays radiation, open the possibility to discover phenomena happening with a very low probability. At present, the main scientific programme at LSC is focussed on direct detection of dark matter and neutrino physics, namely neutrinoless double beta decay. Yet, the LSC is also active in geophysics and biology.

Six experimental complex equipment proposed by groups of users from international universities and laboratories are already working or under commissioning, while more underground space is still available for new proposals.

Laboratories, offices and meeting rooms are also available on the surface.

An exhibition room is in preparation in "La Casa de los Abetos" on surface near the main LSC premises.

The LSC provides at present the following services to users:

- Material radio-purity measurements with very low background HPGe detectors (Ultra Low Background Service, ULBS)
- Radio-pure copper parts manufacturing service using the electro-forming technique (Copper Electro-forming Service, CES).
- A laboratory equipped with an ICP-MS.
- Underground clean room class ISO 6 and class ISO 7 (Clean Room Service, CRS).
- Two Conference rooms for institutional meetings with 95 seats each.

We welcome both new scientific proposals, which can be hosted in the still free underground space and requests for services. The LSC International Scientific Advisory Committee will analyse the scientific proposals, giving its advice to the management based only on the scientific excellence.

The mission of LSC is delivering world-class science and providing international access to a unique research infrastructure.

This Report summarizes the science and the experimental activity carried out in 2017. It is based on the annual reports submitted by each experiment, which have been edited by the LSC. Any inexact element introduced in the editing should be credited to LSC.

Aldo Ianni
Canfranc Estación, April 2018

IN MEMORIAM

((By LSC staff & GIFNA researchers))

Last August 2017 Prof. José Ángel Villar, Joint LSC Director, sadly passed away leaving an empty space at the LSC impossible to be filled.

José ÁngelVillar Rivacoba was the spokesperson for ANAIS collaboration and chair professor of Atomic, Molecular and Nuclear Physics at the Theoretical Physics Department of the University of Zaragoza. He was also Bachelor and Doctor in Physics (PhD Thesis supervised by JulioMorales) by this University.

He joined the Angel Morales's Group of Nuclear and Particle Physics and participated in the first efforts to build an underground facility in Spain, exploring different locations. The Somport tunnel, in Canfranc, under the Pyrenees housed the first underground experiment devoted to the study of the Ge double beta decay around 1985-86 and it would later become the Laboratorio Subterráneo de Canfranc (LSC).

With the group of the University of Zaragoza he participated in relevant experiments internationally in the rare events searches field such us: Neutrino physics (IGEX, Kr-78), Dark matter searches using Ge detectors (COSME, IGEX-DM), NaI (DM32,ANAIS) and bolometers (ROSEBUD) as well as Axion searches (CAST, IAXO).

The IGEX experiment was the most relevant of the experiments carried out in the LSC in the 90's At that time he was supervisor of a PhD Thesis on the double beta + / EC beta + decay of 78Kr , in collaboration with the INR, Moscow.

He co-led the group of Nuclear andAstroparticle Physics at the University of Zaragoza with Julio Morales since 2003 and led it from 2009, after Julio passed away.

He supervised 6 PhD Thesis, was the PI of more than 40 research projects in Spanish National Plans and is the co-author of more than 150 scientific publications.

He was strongly committed to the setting up and commissioning of the new Canfranc Underground Laboratory facilities and was its Joint Director from 2007 to 2017.

He was really proud of the LSC and thoroughly enjoyed guiding visitors through its facilities.

He was also strongly involved in scientific management at both national and international level:

- He was the coordinator of the national network of astroparticles (RENATA)
- Member of the Executive Committee of the National Center for Nuclear and Astroparticle

Physics (CPAN)

- Member of the general assembly and Joint Secretariat of the ApPEC Consortium
- Member of the Board and Science Assembly of ILIAS
- Adviser to the successive Ministries responsible for Science and Technology in Spain, the Government of Aragon and many evaluation agencies

He was part of the organizing committees of many international relevant conferences and workshops. It is worth to highlight the contribution to the TAUP conference series, International Meeting on Fundamental Physics

(Winter Meetings), and the organization of the NEUTRINO 92 conference in Granada.

He also loved to participate in outreach activities of every kind: Conferences for secondary school students and general public. He also collaborated frequently in the "Experience University", for elderly people and was a well-known collaborator in the local press media, he even prepared a scientific documentary film on "Radioactivity".

He was highly regarded as scientist but we will mostly remember him for his quality as a person, his good humor and his endless smile. He will be sadly missed.

1 INTRODUCTION

LSC is a world-class deep underground laboratory designed to investigate neutrino physics, dark matter and rare processes in physics. As of today, LSC is the second largest deep underground laboratory in Europe. Strong synergy with other similar infrastructures is underway at LSC to exchange expertise and put forward common interests.

In the framework of sub-atomic physics, researchers have developed a theoretical description of the elementary building blocks of matter and of the basic forces of Nature, called the Standard Model (SM). We have tested with increasing precision all its predictions at the energies that are reachable with the accelerators. A fundamental element that was missing, the Higgs boson, was discovered at CERN in 2012. Underground laboratories, such as LSC, provide scientific information that is complementary to that obtained in laboratories with accelerators. Indeed, the first element of physics beyond the SM came from underground experiments, namely neutrino oscillations. Science carried out in underground laboratories such as LSC is growing in interest worldwide. There is a strong international competition with new proposed underground infrastructures. Yet, this competition might develop in the future in a worldwide collaboration to reach the ultimate sensitivity for extreme rare processes. Therefore, LSC is collaborating with other similar infrastructures, in particular, with LNGS in Italy, Boulby in UK, and SNOLab in Canada.

Underground laboratories are dedicated to the search for extremely rare nuclear and sub-nuclear phenomena, such as neutrinoless double beta decay and dark matter interactions. This search requires a very low radioactive background environment.

We cannot detect the signals of very rare nuclear decays in presence of the much higher natural radioactivity background, which can be measured on surface. This background noise is due mainly to cosmic rays (see Fig. 1.1), originating from cosmic protons hitting nitrogen or oxygen nuclei in the upper layer of the atmosphere. The proton interaction produces a shower of secondary particles. Among these latter the muons, μ, and neutrinos, ν, are the most penetrating. Muons reach the surface of the Earth with a flux equal to about 2 muons/cm2/sec.

The underground area at a depth of 800 meters (about 2400 meters water equivalent) is excavated between the Somport road tunnel and an abandoned train tunnel about 8 km long at the border between Spain and France. Deep underground, under the Tobazo Mountain near the Canfranc village in Spanish Pyrenees, the cosmic ray flux of muons is reduced by a factor of about sixty thousand. Therefore, the reduced cosmic muons flux allows to search for very low probability processes.

Only about 5% of the matter in the Universe is visible. The rest is of an unknown nature and referred to as dark matter. Understanding the

nature of dark matter is a fundamental goal for modern science. LSC is contributing to this international and fundamental effort.

Fig. 1.1: *Simulation of shower of cosmic rays over Mount Tobazo*

At present, we know that neutrinos have very small masses. A natural explanation for the smallness of the neutrino mass requires them to be Majorana particles. A Majorana particle has the property to be its own antiparticle. If neutrinos are Majorana particles a fundamental parameter, the lepton number, conservation law will be violated. In the SM the lepton number is conserved. Searching for neutrinoless double beta decay can prove that neutrinos are Majorana particles and that the lepton number is not conserved. The lepton number violation may be related to the matter-antimatter asymmetry of the Universe. Again LSC is contributing to this important international research goal.

At LSC these research activities are carried out by a number of different detectors built by international collaborations. In particular, at LSC two experiments on direct detection of dark matter are underway, ANAIS with NaI(Tl) scintillators and ArDM with liquid argon.

A new project, named TREX-DM, on direct detection of dark matter with argon and neon in a high pressure TPC is being installed in Hall A.

The demonstrator of an experiment on neutrinoless double beta decay, NEXT-NEW, is in operation, and a test facility, BiPo, for the SuperNEMO experiment planned in the Modane Laboratory, France, is fully operational. The CROSS project to search for neutrinoless double beta decay with a bolometer based on tellurium or molybdenum is under preparation in Hall B.

Other scientific sectors can profit of the unique location of the underground infrastructures at LSC. Geodynamics research can be carried out underground at LSC with the goal to measure and study extremely small changes in the stress of the rock deep inside the mountain due to very small local seismic or teleseismic events. The enhanced sensitivity underground is due to a significant reduction of the human activity and atmospheric phenomena present on the surface. LSC is equipped with a geophysics infrastructure, named GEODYN. GEODYN is an observatory and covers the whole geodynamic spectrum, from near-field seismicity to tectonic deformations, Earth tides or Earth-core nutation. The facility has three components: seismic station, laser strainmeters and external GNSS stations. The

Fig. 1.2: *The Train Tunnel at LSC*

seismic station and the laser strainmeters are installed underground. The ETSEC project aiming to study the newtonian noise in the framework of gravitational waves detection in underground is in data taking. ETSEC has seismometers deployed along the train tunnel (four) and two in one by-pass tunnel between the train tunnel and the road tunnel.

In addition, LSC and the long train tunnel (see Fig. 1.2) offer the possibility to carry out studies on subsurface microbiology to understand, as an example, what processes regulate the energy flux for life underground. The GOLLUM project at LSC is interested in the identification and characterization of the microbial communities living in a range of different rocks throughout the length of the train tunnel.

In conclusion, LSC is a multidisciplinary world-class science infrastructure with 1600 m2 surface and a total volume of 11000 m3 in underground equipped with a number of service facilities to support research activities performed by international collaborations. The main underground infrastructure, named LAB2400, is divided in Hall A (Fig. 1.3), the largest experimental area, and Hall B. The other infrastructures are named LAB2500 and LAB780, respectively. At LSC international collaborations are carrying out research at the frontier of particle physics and particle astrophysics. A possible upgrade for LSC in the coming years could come through a new excavation to build an infrastructure for nuclear astrophysics or an instrumented water tank, which works as an active muon veto for a next generation experiment.

Fig. 1.3: *Hall A at LSC (2017)*

2 REPORT ON ACTIVITIES AT LSC IN 2017

The following experiments have been carrying out activities at LSC in 2017: ANAIS and ArDM (a CERN Recognised Experiment) on dark matter, NEXT-NEW (NEXT100 demonstrator and a CERN Recognised Experiment) on neutrino physics, GEODYN and ETSEC on geophysics. Two other projects have been in operation as ancillary set-ups to experiments in other laboratories: BiPo for the SuperNEMO proposal at the LSM laboratory near Modane in France and SUPERKGd for the Super-Kamiokande experiment in Japan.

Preparation work for the CROSS experiment on neutrinoless double beta decay with bolometers based on tellurium and molybdenum has been carried out.

In addition, the new experiment, named TREX-DM, is about to be installed in Hall A (See Fig. 2.1). TREX-DM is a high pressure TPC in a copper vessel filled with less than 1 kg underground argon (depleted in 39Ar) or neon to search for dark matter interactions. Risk assessment work has been carried out for TREX-DM to allow commissioning and operations as soon as the installation is completed.

Fig. 2.1: *Cleaning of lead in preparation for the installation of TREX-DM in Hall A*

The GEODYN infrastructure at LSC has three components: seismic station, laser strainmeters and external GNSS stations. The seismic station and the laser strainmeters are installed underground. The seismic station is equipped with a Titan accelerometer and a Trillium 240s seismometer.

The laser strainmeters consist of two independent and orthogonally oriented 70 m long tubes under vacuum. The LSC GEODYN observatory has been integrated in the European Plate Observing System (EPOS), which was approved by the ESFRI Roadmap in 2008. In 2016 the strainmeter in LAB780 (See Fig. 2.2) was put back in operation. In

Fig. 2.2: *Strainmeter at Lab780*

2017 both strainmeters have been in data taking.

Due to the profile of the mountain at LSC the muon flux underground is expected to show an angular distribution. In order to study this, a muon detector was installed and run in Hall A for more than one year. Later the detector was moved to LAB2500, where another year of data has been taken. Data hand results have been reported in a publication.

Measurements have been performed with a CLYC scintillator in Hall A (Fig. 2.3). This effort, named CLYC-N, aims to make from a CLYC scintillator a detector to monitor radiogenic neutrons in underground laboratories. This work is carried out in collaboration with CIEMAT.

Fig. 2.3: *CLYC-N detector in Hall A*

The ULBS Service at LSC has been in operation since 2010 in Hall C in LAB2400. The ULBS is offering a high quality screening facility to experiments. At present, it is equipped with seven p-type coaxial High Purity Germanium (HPGe) detectors (Fig. 2.4). Each detector is shielded with 20 cm of lead with a low contamination in 210Pb. An internal OFHC copper layer completes the shielding.

In 2017 the ULBS has carried out radio-purity assay for experiments working at LSC. In addition, a new characterization of a SAGe detector has been completed and shared with the supplier to enhance the sensitivity of the apparatus to be used at the LSC. This work is still underway.

Fig. 2.4.: *HPGe detectors in Hall C*

The CES Service at LSC is a unique facility amongst the underground laboratories in Europe. This Service got interest to carry out research to understand the surface contamination due to 210Pb and 210Po, and to characterize the properties of electro-formed copper for low temperature use in bolometers. In 2017 an effort has been done to use the facility to study the surface contamination on electro-formed copper. This work is done in collaboration with the Jagiellonian University in Krakow.

Environmental measurements (radon, temperature, humidity, atmospheric pressure, water radioactivity contamination) have been carried out in collaboration with the LABAC (Laboratorio de Bajas Actividades) from the University of Zaragoza both underground and on surface at LSC.

Two meetings with GLIMOS took place in 2017 to review safety procedures and interactions between users and LSC in matter of safety.

At LSC a monitoring system is in operation to study rock deformations underground. Specifically, LAB2400 is equipped with a system of optic fibers to monitor any

deformation of the vault, which might occur in the underground site. Optic fibers are deployed in 10 locations: 4 in Hall A, 2 in the corridor, 1 in Hall B and 3 in the area outside the main entrance. In addition, a monitoring of the convergence (distance between fixed points) is carried out every month by means of calibrated rods for a number of specific points. In 2017 a new system to monitor cracks on the floor of Hall B has been installed.

In the following we report about new infrastructures installed and upgrades carried out at LSC in 2017.

The infrastructure at LSC has been upgraded with a radon detector with sensitivity of order 1 mBq/m3. This system is installed in Hall A on a new platform built close to the entrance. The detector is under commissioning. This detector will be used to monitor the radon-free air delivered by the radon abatement system (see Fig. 2.5) and to monitor radon contamination in sensitive parts for NEXT, ArDM, BiPo and, TREX-DM. The radon detector has been put in operation and calibrated. A distribution line to delivery radon-free air inside the shielding of NEXT-NEW has been installed.

Fig. 2.5: *Radon abatement system*

The LSC monitoring system (Slow Control) has been upgraded in order to improve the general SCADA interface and alarms, to design and store a database, and to include some external building parameters.

It also included a crack width measurement in different points of the lab, especially in Hall B. The system has 5 points of measurement in Hall B and in the corridor. With this system, the lab controls the movement of different cracks in both axels.

Also we started the installation of the new detection fire system in Halls A and B. The new system is an aspiration system. In 2017 we installed the pipes of this system in both Halls. This system will be concluded in 2018.

The LSC has been upgraded with a new instrument, namely an ICP-MS (see Fig. 2.6), to perform radio-purity assay. The ICP-MS has been installed in the LSC main building.

Fig. 2.6: *ICP-MS at the Chemistry Lab in the Main Building*

The CLYC detectors as well as the ICP-MS the Radon Detector, installed in Hall A, have been cofounded in a 50% by FEDER (Fondo Europeo de Desarrollo Regional within the "Programa Estatal de Fomento a la Investigación Científica y Técnica de Excelencia" in the frame of the "Plan Estatal de Investigación Científica y Técnica y de Innovación".

A new building named "La Casa de los Abetos" was given to LSC in 2015. The building is located just outside the surface building of LSC in Canfranc Estación. In 2017 the exhibition room in "La Casa de los Abetos"

Fig. 2.7: *Muon detector at the "Casa de los Abetos"*

was almost completed and equipped with a muon detector (see Fig. 2.7), a detector to measure the meanlife of cosmic muons, and screens for divulgation about the underground laboratory.

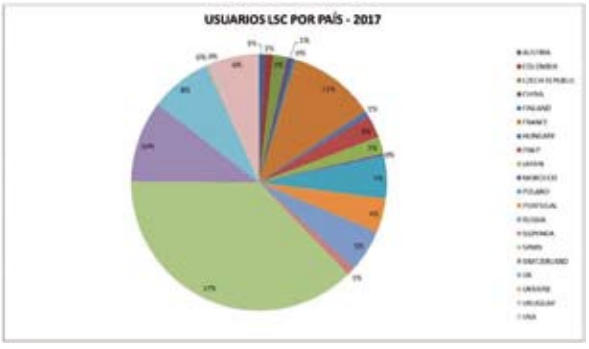

Fig. 2.8: *LSC users by Country in 2017*

The total number of users in 2017 has been 281, from 20 different countries (Fig. 2.8).

The LSC is running a programme of visits, with over 2000 visitors in 2017. In Fig. 2.9 we show the trend of visitors at LSC during the last eight years.

Fig. 2.9: *Records of visitors at LSC spread over the last eight years*

3 RECORD OF EVENTS IN 2017

Workshop on Double Beta Decay (7-8 February 2017)

The LSC Director called a workshop on Double Beta Decay which took place at the LSC facilities on February 7-8.

This workshop had a double objective, firstly the revision of the radon background problem of the NEXT experiment, carried out by a panel of experts, and secondly attracting interest for a future development/support to this experiment.

The invited professors also gave talks related to double beta decay

Meeting of the "Consejo de Turismo de Aragón" (3rd of March 2017)

On Friday 3rd of March, the facilities of the Laboratorio Subterráneo de Canfranc held the annual meeting of the "Consejo de Turismo de Aragón" chaired by the "Consejero de Vertebración del Territorio, Movilidad y Vivienda", José Luis Soro.
This meeting took place at the auditorium located at the LSC headquarters building.

Meeting for the review of the Risk Analysis of the NEXT-NEW gas system (8-9 March 2017)

The LSC director called a panel of experts from different institutions for the second review of the Risk Analysis of the NEXT-NEW gas system and the development of a report issued after this meeting.

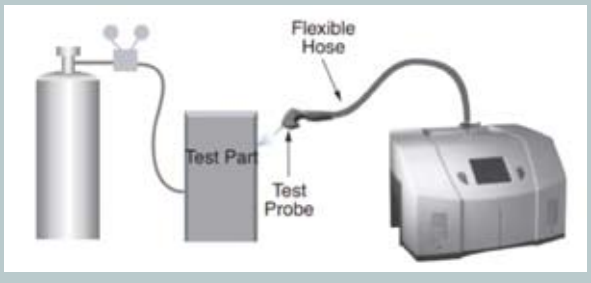

NEXT Collaboration Meeting (9-11 of May 2017)

Around 40 researchers from the NEXT collaboration met at the LSC facilities in Canfranc to carry out one of the annual meetings of this collaboration.

20th LSC Scientific Committee Meeting (11-12 May 2017)

The Scientific Advisory Committee is composed of scientist of international reputation. It gives advice on experimental proposals and monitors the progress of the approved experiments. On this meeting, the Committee had a presentation from a specialist firm from Zaragoza on the benefits of an electromagnetic survey of the lab and of equipment that might be located in the lab.

CANFRANC BIM - EUPLA Architecture Course (3-7 July 2017)

Summer course of the University of Zaragoza organized by EUPLA (Escuela Universitaria Politécnica de La Almunia). This summer school on the topic of architecture was held in the LSC's "Casa de los Abetos" with the attendance of 15 students whom studied the structure of the building which holds Canfranc's Railway Station and modeling in 3D.

Open Day (19 November 2017)

The LSC organized an open day for the general public to visit its premises. Around 120 people took part on this visit which included a public talk on the history and present story of the lab, access to the underground facilities and a specialized talk on Gravitational Waves by Prof. Martin Obergaulinger from the VIRGO group of the University of Valencia.

21st LSC Scientific Committee Meeting (23-24 November 2017)

The Scientific Advisory Committee is composed of scientist of international reputation. It gives advice on experimental proposals and monitors the progress of the approved experiments. This meeting commenced with a talk by Maria Luisa Sarsa, form the GIFNA group, remembering the late LSC Associated Director José Ángel Villar who sadly passed away in August.

Presentation of the studies for the Opening of the Canfranc-France railway tracks – (1st December 2017)

Canfranc made history holding the signature of the grant agreement between Spain and France of the European grant agreement on 7,5 million euro to carry out the final studies for the re-opening of the international railway line (closed since 1970). The end of these studies, subsidized by the European Union, is foreseen towards the end of 2020 so the works which will allow the re-opening of the Canfranc train can start. These agreement was signed at the LSC premises by the presidents of Aragon, Javier Lambán, and Aquitania, Alain Rousset, together with Herald Ruijters, director of Innovating and sustainable transport of the EU.

4 SNAPSHOTS

Visit of APPEC Chairman, Antonio Maseiro. February 2017

Visit of José Luis Soro, Consejero de Vertebración del Territorio, Movilidad y Vivienda de la DGA. March 2017

Visit of Carmen Vela, Secretaria de Estado de Investigación, Desarrollo e innovación. May 2017

Broadcast of the radio program "Agropopular" from the LSC. January 2017

Presentation of the Muons's Telescope at the Researcher's Night Zaragoza. September 2017

5 ANAIS
THE JOURNEY OF THE EARTH AND DARK MATTER

http://gifna.unizar.es/anais

ANAIS is a project to search for dark matter looking for the annual modulation of the counting rate expected as a characteristic signature of the galactic dark matter. There is only one experiment that has reported positive evidence so far, DAMA/LIBRA at Gran Sasso underground laboratory (LNGS) in Italy. Such an evidence has never been confirmed by experiments with much larger sensitivity all over the world. However, this apparent contradiction cannot be considered definitive, because different techniques and different target nuclei have been employed. A confirmation or refutation of the DAMA/LIBRA positive result can only come in a model independent way by using similar detectors, namely NaI scintillating crystals, in very low background and low energy threshold conditions. A few experimental efforts in the world are pursuing this same goal.

At the end of 2016, six out of nine of the ANAIS modules were already in the Canfranc Underground Laboratory (LSC). D4 and D5 detectors, funded by LSC, had just arrived and were taking data for performance assessment. The purchase order to Alpha Spectra Company (AS) for the last three modules was issued on December 2016, funded by MultiDark project. ANAIS electronics had been tested and installed inside a temperature-controlled space at LSC Hall B, and shielding materials, as well as the muon veto plastic scintillators, were ready for installation in the ANAIS112 set-up.

The last three AS modules, D6, D7 and D8 (shown in Figure 5.1) were grown with the WIMPScint-III quality powder, which should have the best potassium content achieved by

Fig. 5.1. *Last three ANAIS AS modules, 12.5 kg of NaI(Tl) each, received in March 2017 (D6, D7 and D8), completing the 3x3 matrix of detectors ANAIS112 consists of.*

AS Company. The crystals were encapsulated following similar protocols and using same materials as in the building of previous modules: OFE copper, synthetic quartz windows, an aluminized Mylar window to allow low energy calibrations, etc.

They arrived to Canfranc on March 2017. Photomultiplier Tubes (PMTs) were coupled at LSC clean room just after reception (see Figure 5.2) and

Fig. 5.2. *Coupling of the PMTs to D6, D7 and D8 modules at LSC clean room, March 2017.*

the mounting in the ANAIS hut at Hall B was done in less than one week. The new modules showed an excellent optical quality, see Figure 5.3. Works on the ANAIS112 shielding had started before, in January 2017: lead and electroformed copper cleaning, conditioning of the ANAIS hut for ANAIS112, testing of the plastic scintillator vetoes, etc.

Fig. 5.3. *Detail on D6 module transparency at LSC clean room, March 2017.*

ANAIS112 consists of a 3x3 matrix of 12.5 kg NaI(Tl) modules, amounting a total mass of 112.5 kg. See Figure 5.4 for an artistic view

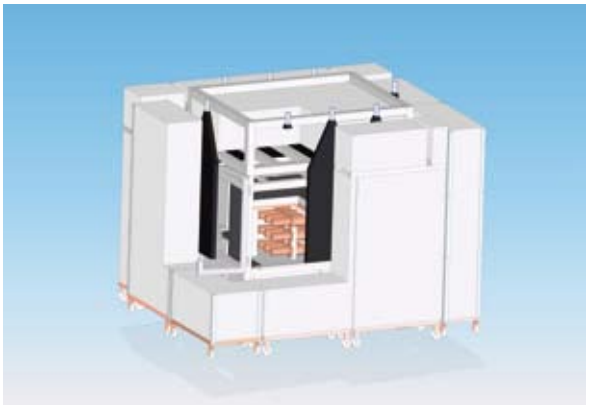

Fig. 5.4. *ANAIS112 artistic view.*

of the experimental set-up and a picture of the modules layout is shown in Figure 5.5. The shielding was commissioned along the first months of 2017 and first tests of all the nine modules were carried out from March until July 2017. After solving some problems with a few of the PMT connections, all the

Fig. 5.5. *ANAIS112 setting-up at LSC: view of the modules layout and calibration system.*

modules were operative during June and July 2017 for calibration and general assessment. The sixteen plastic scintillators forming the ANAIS112 active veto system were installed in May 2017, together with a metallic structure to partially support the neutron shielding (see Figure 5.6). Neutron shielding was

Fig. 5.6. *ANAIS112 set-up before completing the neutron shielding. Plastic scintillators vetoes, installed in May 2017, can be seen.*

installed in July, in several steps, and it allows partial opening for periodical calibrations. The neutron shielding consists of water tanks and polyethylene bricks, amounting 40 cm thickness in total (see Figure 5.7).

The low energy calibration system, consisting of Cd-109 sources in a flexible wire that can be positioned just in front of the Mylar window of each module, is working properly and all the nine modules are calibrated at the same time.

Outstanding high light collection has been determined for all the modules, at the level of 15 photoelectrons/keV, which is twice the best light collection published for DAMA/LIBRA modules.

Alpha specific activities for the three new modules were determined by Pulse Shape

Fig. 5.7. *ANAIS112 set-up after completing the installation of the neutron shielding in July 2017.*

Analysis selection of the high-energy events providing values of 0.80, 0.78 and 0.74 mBq/kg for D6, D7 and D8, respectively. These values are consistent with those of the best modules manufactured at AS. Profiting from the high modularity of ANAIS112 set-up, efficiencies for K-40 coincidence detection, determined by Geant4 Monte Carlo simulation, are much higher than in previous set-ups allowing for a better determination of the crystal potassium content. Potassium content for D6, D7 and D8 modules is, respectively, 28, 31 and 22 ppb.

The ANAIS112 Dark Matter (DM) run started on August the 3rd and data taking will continue uninterrupted for at least two years, being the data in the region of interest blinded since then. The data taking has been progressing very smoothly from August to December 2017 and one of the most important assets of ANAIS112 in the search for the annual modulation is the very high duty cycle expected. In Figure 5.8 we show the percentage of live/dead/down time along the ANAIS112-DM run, from August the 3rd until November the 2nd, 2017 (first three months of data taking in DM mode run).

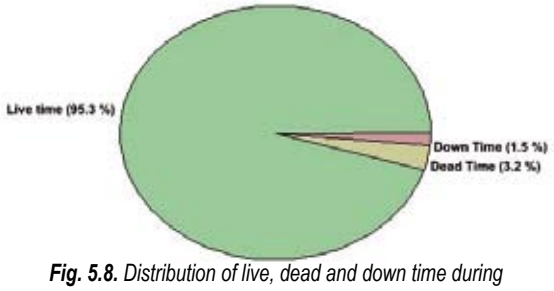

Fig. 5.8. *Distribution of live, dead and down time during the first three months of ANAIS112 DM run, from August the 3rd until November the 2nd, 2017.*

We worked very hard in the first half of 2017 to have ready the monitoring of environmental parameters before the start of ANAIS112 DM run. It consists of several windows for monitoring N2 gas flux entering into the shielding; temperatures at electronics, inner shielding, laboratory, preamplifiers, etc.; radon content in laboratory air; relative humidity; HV supply to every PMT; muon rates; etc. (see Figure 5.9). The system saves all the data every few minutes and alarms have been set on the most relevant parameters sending alarm messages through Telegram.

The ANAIS112 data taken while the commissioning run, from March to July 2017, have been analysed to understand the relevant background sources in the three new modules. Figure 5.10 presents the background spectra at the low energy region. First and latest data are compared, showing the decay of cosmogenics in the last received detectors. Preliminary background models for those modules (see one example in Figure 5.11 for D8 module), considering the measured crystal and other detector components activities and the ANAIS112 configuration, point to same

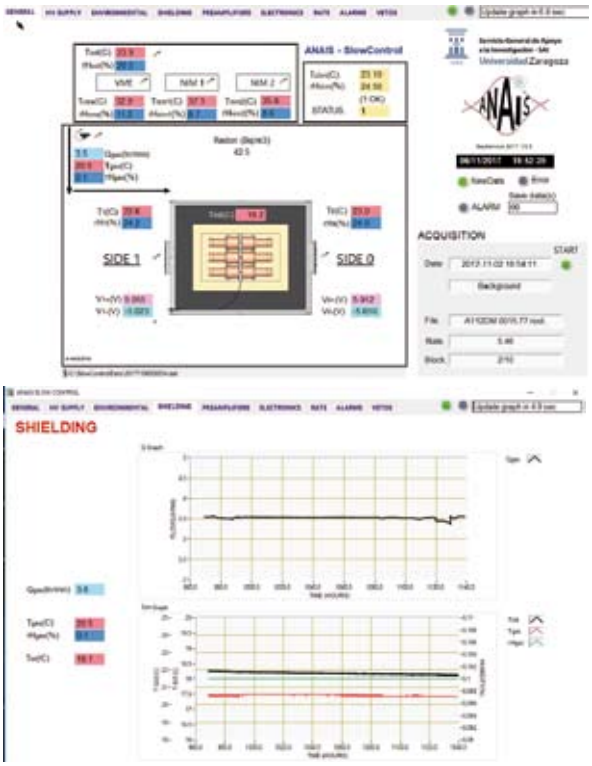

Fig. 5.9. Environmental parameters control windows.

relevant background sources in the very low energy region than in previous modules.

ANAIS112 sensitivity allows exploring in five years of data taking the singled-out by DAMA/LIBRA parameter space of dark matter particles at three-sigma level. Status and prospects of the ANAIS experiment have been published in international journals and presented in important conferences of the dark matter detection and underground physics fields, as TAUP conference series (held in Sudbury, Canada, in July 2017).

Professor José Ángel Villar, ANAIS spokesperson, passed away in August 2017. Serve these lines to express the deep sorrow of ANAIS research team and to remember José Ángel contribution to ANAIS112.

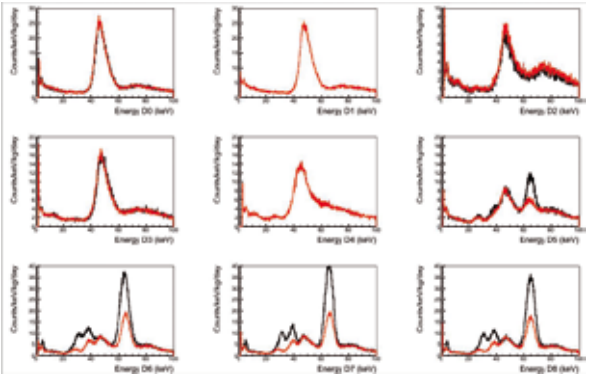

Fig. 5.10. Low energy background spectra in ANAIS112 commissioning run; first and latest data in the period are compared, showing the decay of cosmogenics in the last received detectors. They correspond to filtered spectra but without cut efficiency correction yet.

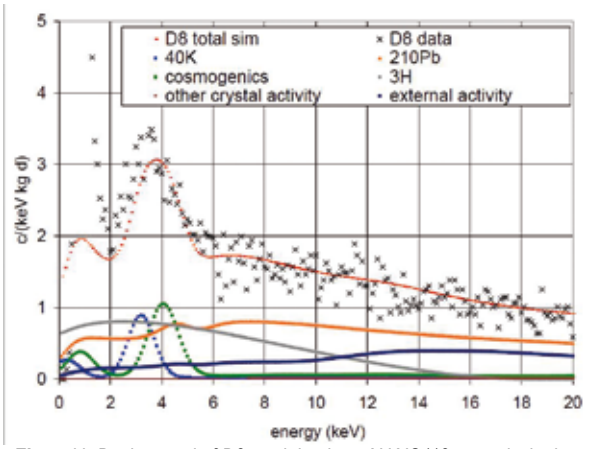

Fig. 5.11. Background of D8 module along ANAIS112 commissioning run at very low energy together with the estimates derived using the preliminary background model.

6 ArDM
LIQUID ARGON AND DARK MATTER

http://darkmatter.ethz.ch/

The ArDM (Argon Dark Matter) Experiment is the first tonne-scale dual-phase liquid-argon (LAr) time projection chamber (TPC) designed for Dark Matter searches, operating at a deep underground site. The detector is designed for the detection of nuclear recoils induced by Weakly Interacting Massive Particles (WIMPs), hypothetical particles that are thought to constitute the Dark Matter in the universe. The ArDM setup, installed in Hall A of LSC, is rendered in Figure 6.1 with the inset depicting the schematic of a WIMP detection in the ArDM LAr-TPC. WIMPs, elastically scattered off argon nuclei, are detected by scintillation light and ionisation charge from the interaction of the recoiling nucleus in the liquid argon.

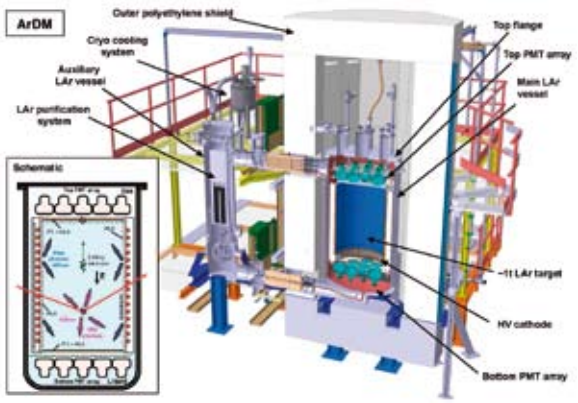

Fig. 6.1: *The ArDM setup with its main components installed in Hall A of LSC. The inset to the left depicts the principle of a WIMP detection in the ArDM dual-phase LAr-TPC. WIMPs elastically scattered off argon nuclei are detected by scintillation light and ionisation charge from the interaction of the recoiling nucleus in the liquid argon.*

The detector was successfully commissioned in single-phase in 2015 (ArDM Run I) and operated with the full LAr target of ~850 kg over six months in stable conditions, recording more than 3x109 primary scintillation (S1) signals. Raw data files are transferred to CERN (Geneva), to be analysed exploiting the local computing infrastructure . Results were reported in three papers [1–3], as well as in a successful PhD thesis [4]. A fully satisfactory understanding of the data was achieved, in particular the detector response and the observed backgrounds. This provided the base for an upgrade of the experimental setup and the transition to the dual-phase operational mode in 2016/17. During the second half of 2017 the ArDM setup was cooled down and initially characterised with a cold gaseous-argon target. Radon emanation rates of the detector and newly developed cleaning cartridges were determined. The filling of the main vessel with LAr started in November 2017 with a first operation in dual-phase mode in December 2017, the start of ArDM Run II. This fact yields a major milestone in the ArDM experimental program.

In 2017 large progress was achieved towards the planning and coordination of future LAr Dark Matter projects. The four collaborations pioneering the developments in this sector (ArDM, DEAP-3600, DS-50, MiniCLEAN) expressed their interest in a white paper [5] to join forces in the framework of a Global Argon Dark Matter Collaboration (GADMC). DarkSide-20k, a dual-phase LAr TPC at LNGS (DS-20k), was identified as the next step in this programme, featuring a fiducial volume of 20 tonnes to reach a sensitivity of 1.2×10−47cm2 at a WIMP mass of 1TeV/c2 in a 100 tonne year exposure. Crucial prerequisites are large quantities of LAr,

depleted from the β-emitting isotope 39Ar. This will be achieved by collecting the argon from deep gas wells with subsequent cleaning (distillation). It is mandatory to characterise individual argon batches. The ArDM setup at LSC was identified to be an ideal facility for depleted argon research and was integrated as a R&D project in the experimental programme of DS20k, strongly supported by the directorate of LSC. Depleted argon tests (DART/ArDM@LSC) are planned for 2018 and beyond.

In the following sections we detail the commissioning of the ArDM setup for dual-phase operation and show some results of the very first Run II data. We also describe the plans for the first step for depleted argon tests at LSC (DART/ArDM) with a small 1Ltr chamber placed in the centre of the ArDM setup, which is currently under preparation.

Commissioning of the ArDM setup for operation in dual-phase

After upgrades of the ArDM detector in 2016 with the newly built drift cage for dual-phase operation, a series of hardware add-ons and inspection work had been carried out in 2017, including a new gas recirculation line, the argon filling system, as well as upgrading and overhauling of the ArDM control system.

The measured light yield during ArDM single-phase operation, suggesting the presence of impurities in the LAr, required an upgrade of the (external) purification system of the setup, which could also be used for purifying the main LAr target during operation. A LAr extraction tube was installed in parallel to the existing GAr connection in the top of the detector and connected to the gas recirculation circuit through a double-wall vacuum insulated pipe. In the new circuit, LAr can be evaporated and warmed up by means of the heating bands installed in the first section of the recirculation line. A speed regulation system for the gaseous recirculation pump, based on an electronic inverter, was added into its AC power line allowing to regulate the gas flow by the ArDM control system.

In order to improve the purity of the LAr ab initio, the detector was filled from boil off argon from low pressure external LAr tanks instead of GAr bottles. The LAr inside the tank was firstly evaporated and then filled into the detector main Dewar via filters. This avoided the impurities in the GAr entering the main Dewar.

The new argon filling circuit realized that design. It consists of four main parts: the portable 600-liter low pressure LAr tank, one evaporator, three purification cartridges, and two motorized electric valves (see Fig. 6.2). The LAr tank, together with the LAr, was supplied by the company LINDE,

Figure 6.2: *Evaporator and motorised valves (left), filter components (middle) and LAr tank (right), used for the filling of nearly 1.5 tonnes of LAr of the ArDM target.*

1 ArDM is a CERN Recognised Experiment (RE18).

Spain. The LAr evaporator was built from a copper tube equipped with 8 electric heaters. The three purification cartridges included one commercially available gas filter (WAFERGARD®III NF-75O in-line Gas Filters) and two custom made cartridges filled with copper wool and charcoal powder respectively. The two cryogenic valves were ordered from Swagelok equipped with electric valve actuators from the German company GULEX. The entire filling circuit was connected through all-metal components, which minimizes the possibility of argon pollution during filling.

All the components and hoses were heat insulated using synthetic rubber insulation materials (ARMAFLEX) to reduce heat input from the environment. The filling circuit was connected to current argon gas recirculation circuit right before the input valve via a VCR-T. This allowed to purge the filling circuit through the venting valve in the argon gas recirculation circuit during cooling the filling circuit.

In parallel to the main detector upgrades, both, the software and hardware of the ArDM control system has been inspected and upgraded in order to support the new argon filling procedure and also to improve the reliability of the experiment. Several temperature sensors were fixed or replaced, on the top flange and in the LAr recirculation pipe and others. Especially the cryocoolers, crucial for flawless operation of ArDM, were overhauled, broken temperature sensors were replaced by more robust electric heaters and heat sinks improved. The parameters of the PID controller were tuned during the system cool down to achieve highest stability of the cryogenic system. To get more precise information about the LAr levels in the bath and Dewar, new level meter readout electronics was built and calibrated. The pressure sensors on Dewar, bath and the argon filling pipe were also re-calibrated. This provided more accurate information about the cooling and filling process. In order to control the argon filling procedure, new temperature sensors and pressure sensor were installed in the argon filling circuit as mentioned before, together with analogue and digital I/O modules, which read out the values from the sensors and regulate the filling valve and the input valve. All the functions were integrated in the current control system.

At September 27th 2017, the cool-down of the experiment was started after several months of evacuation and flushing of the main Dewar. Starting from room temperature, GAr was condensed inside the experimental cooling bath from the external bottles with the aid of all the three cryocoolers. At the same time, the whole tank, including the massive stainless-steel structure of the system and the neutron shield inside the tank, was cooled to cryogenic temperature. After the system was cooled down, one cryocooler was turned off at October 5th, and the electric heaters started working at regulation mode. The PID parameters had been tuned to keep the temperature and pressure inside the bath and the Dewar stable. Since then, the detector had been operated with the cold argon gas target.

The filling of the main Dewar started at November 8th 2017 by means of boil-off argon of the delivered LAr. The temperature stabilised evaporator (100 K) acts as a safety device that the liquid argon cannot reach the

filling circuit and hence the filters. It supplies the necessary heating power according to the gas flow. Passing through the two purification cartridges and the particle filter, the clean cold argon gas is fed to the ArDM main vessel. The gas flow is controlled by the opening of a motorized filling valve which is regulated by the pressure before the charcoal filter to maintain it at a fixed level (~0.5 barG). In this way the gas flow is well controlled by the impedance of the filtering system and the system runs very stable. Finally, the cold argon gas is condensed in a heat exchanger inside the ArDM cooling tower. The whole process was regulated by the ArDM control system and monitored by shift personnel. Filling of the ArDM system was also monitored by the increasing trigger rate due to the increase in target size. The functionality of the internal LAr cleaning system was observed from the lifetime of the slow scintillation component (compare Fig.3 right in next section).

After the detector was fully filled on December 1st 2017 the charge extraction system was aligned to the liquid argon surface (precision of ~0.25mm) and adjusted to form a gas gap of about 6mm above the LAr level. Following these adjustments the electric fields for drift (100-300V/cm) and extraction (~4kV/cm) could be applied and configured through the ArDM control system. The immediate presence of S2 signals was observed on the oscilloscope, as well as by the increasing trigger rate (2 signals per event). Generally a high stability of the HV systems was observed, leakage currents were below the detection limits (nA). The extraction field influences charge extraction probability, as well as the luminescence in the gas.

The size and homogeneity of the fields are crucial for dual-phase operation and the precise adjustment of the liquid level and the alignment of the grid-anode assembly play an important role. These parameters are among the most crucial for dual-phase operation and are subject to tuning. Additionally also the trigger and DAQ systems have to be adapted to the higher rates and the length of the S2 signal due to the much longer light tail from the scintillation in gaseous argon. Since December 2017 ArDM is running in dual-phase mode and keeps taking data while these parameters are being optimised.

Basic performance in dual-phase operational mode

During the preparation for Run II and first data-taking periods, November and December 2017, our focus was set on monitoring and

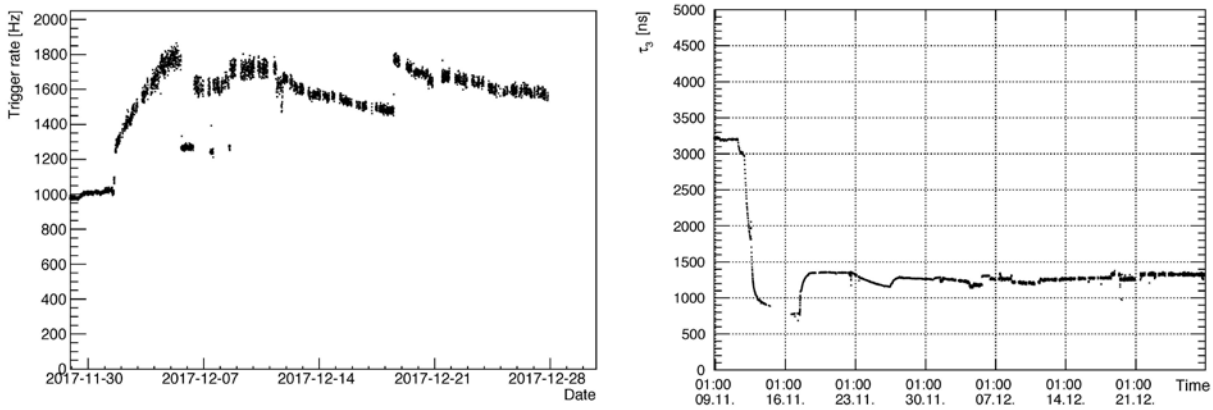

Figure 6.3. *Trigger rate and measurement of the slow scintillation decay time component during filling*

tuning of the filling and dual-phase operation conditions. At the same time the simulation framework for the new setup and S2 signals was prepared.

In the case of dual-phase operation the trigger rate in ArDM increases substantially with respect to single-phase mode. The ArDM DAQ system has been prepared for data taking up to 3.4kHz rate, and the trigger rate was monitored during the employment of various drift and extraction fields, as shown in the Fig.6.3 left. The following can be observed: after a trigger rate of ~1.2kHz has been established (2017-12-01) in single phase mode (stemming mainly from the S1 signal rate of 39Ar in the target), the gradual adjustment of the drift field between 120 and 240V/cm, and extraction fields in the order of 3..4kV/cm, produced an increased trigger rate varying between 1.4-1.8kHz (time scale up to 2017-12-06). This was followed by a period of further adjustments and testing of the system in single and dual-phase modes. From 2017-12-12 until the end of the year ArDM was running stable in dual-phase mode at a nominal drift voltage of 180V/cm. The extraction parameters have been set in the following way: the transparent conductive anode (ITO coated PMMA) has been kept at 0V, while 10mm below this surface the extraction grid was held at -3.2kV, and subsequent field shaper rings such as the top copper ring and the first field shaper ring were held at -3.8kV and -4kV, respectively. On 2017-12-18 the extraction grid and copper ring potentials have been further adjusted, in order to increase the extraction field, to -3.8kV and -3.9kV, respectively, as a result of which the trigger rate increased to ~1.8kHz. A slow decrease in the trigger rate over longer periods was found and attributed due to a slow decrease in the settling liquid Argon level.

The basic performance of a dual-phase mode operation has been also confirmed monitoring the distribution of the vertical localisation variable (TTR = Top to Total light signal ratio, Total = Top + Bottom PMT signals, see our last reports) versus the F90 variable (F90 = ratio of light signal in the first 90 nanoseconds to the light signal in the whole 4 microsecond integration window) between the two data taking conditions: in single- and dual-phase modes. In single phase mode the events are distributed along the vertical position more or less homogeneously, their boundaries defined by the position of the top and bottom PMMA plates, and with a mean characteristic F90 value of F90 ~ 0.35, according to the Component Ratio expected from data dominated by Electron Recoil events. In contrast, in dual-phase mode there is an excess of events which populate the very low F90 values and their mean vertical position is found to be above the single phase maximum TTR value – such events are expected from secondary electroluminescence light emission of electrons having drifted to the liquid Argon level, extracted to the gas Argon phase, and accelerated due to the presence of a large electric field. The decreased F90 value is also expected for secondary light emission events due to the relatively long drift time in the gas (1μs), random collisions in the gas phase and the long decay time of the scintillation light in gas (~3.2μs). The observation of these excess events at the top of the liquid level, and with different F90 value, shows clear evidence for

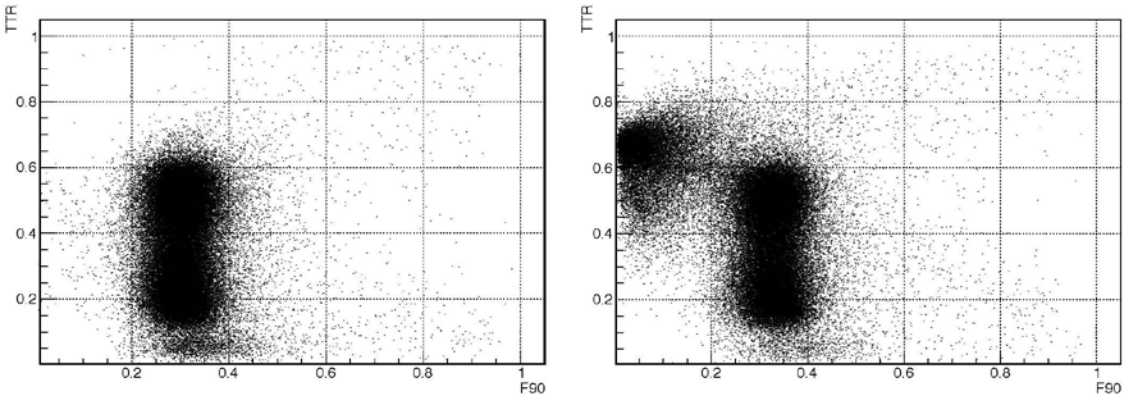

Figure 6.4. *The onset of S2 events in the upper part of the ArDM detector in case of applying the HV for charge extraction is clearly seen in the right plot (HV on) versus left (HV off).*

the successful dual-phase mode operation of ArDM (Fig.6.4).

The liquid Argon purity has also been monitored by recording the mean triplet excimer lifetime for each run during the liquid Ar filling, single and dual-phase mode data taking periods. Figure 3 right shows the observed lifetime accross 2 months. The initial lifetime of ~3.3 microseconds was measured at the end of the cold gas commissioning period, just before starting the liquid argon filling procedure into ArDM. The lifetime then gradually dropped until about middle of November 2017 (due to the increasing liquid level and the shorter lifetime in liquid ~1.6μs) at which point the internal liquid Argon pump was employed for cleaning the liquid through an internal copper cartridge filter. This increased the liquid Argon purity to around 1.4 microseconds, after which, apart from small variations due to various standard operations, the monitored triplet excimer lifetime stayed basically stable. The LAr triplet lifetime (from the scintillation signal) does only give a rough indication about the electron lifetime during drifting in the liquid phase, the latter being an important measure of the performance during dual-phase mode. However, considering the fact that in dual-phase mode the trigger rate increased by ~50% without any sophisticated tuning of the extraction field (optimising trigger thresholds for S2), and assuming a nominal electron drift velocity of ~1.5mm/μs in the liquid, it is expected that the electron lifetime is in the order of at least a few hundred microseconds. This is also in agreement with rough estimates on the correlation between signal heights versus their vertical position in the LAr target.

During the analysis of data from ArDM Run I the results showed that both internal and external Electron Recoil backgrounds considered give a fully satisfactory description of the features found in the single-phase mode data. The further development of ArDM software and simulation codes have started during 2017 in order to prepare the analysis for processing and understanding the ArDM Run II data. The new geometry has been fully incorporated into the Geant4 detector model. Preparations for the treatment of the dual-nature of events (primary and secondary triggers) have been started, and the modelling of the secondary light emission has started as well. The next step is the collection and analysis of large scale of data and validation of the software and simulation using the Run II single and dual-phase data.

Figure 6.5: *ArDM central detector with the ~1Ltr DART*

Towards depleted argon tests at LSC in the framework of DART/ArDM

In future, the low background ArDM installations will be used for a critical development for the next generation LAr DM projects in the framework of the DS-20k programme. In 2017 a task group (DART) was formed with regular weekly meetings to develop the experimental path for such activities. The first phase of DART consists of constructing a small single-phase LAr chamber, containing about 1 kg of test argon, to be operated inside the main ArDM apparatus. In this configuration ArDM will operate in single phase mode as an active veto for internal and external background radiation. The first goal is to measure the intrinsic remnant contamination, particularly the 39Ar and 85Kr contents, of the argon recuperated from the CO2 gas well of the Kinder-Morgan plant, Colorado (USA). Mass production of depleted argon is under way but still needs the installation of additional components at the gas extraction plant. In order to achieve a good sensitivity to the 39Ar depletion factor (expected sensitivity ~1mBq/kg at a 5σ level at a few days exposure) it is of utmost importance to minimize background sources. We are currently designing the small OHFC vessel (inner figure in the montage of Fig. 6.5), which will host two tiles of 24 SiPM, placed inside on top and bottom of the small vessel. The tiles are of the same type as the ones used in DS-20k (prototypes).

Even though we are planning to carry out a first test with the SiPM mounted on standard FR4 substrates, we are investigating possible alternative more radiopure options for the tile substrate. Preliminary screening results confirmed that Arlon is a viable option for the purposes of DART. Samples of Arlon were ordered and are currently under study. The active volume of the chamber is delimited by a reflector foil coated with the wavelength shifter TPB (tetraphenyl butadiene) deposited by evaporation, similar to the type used in ArDM. The internal structure is fixed to the copper cap of the chamber. Two 1/2 inch copper tubes are used to circulate argon through the chamber, as well as to route the signal wires from the tiles to the electrical

feed-throughs placed on the ArDM top flange. The chamber will be constructed such that the mechanical stability is sufficient to allow its evacuation during operation of the ArDM main vessel (minimum wall thickness 5mm). Simulations show that the efficiency in tagging the gamma background radiation is reduced as we increase the thickness of the walls, since the copper can stop low energy gammas. For this very same reason, thicker walls can act as an extra passive veto to external radiation. The optimal thickness is under study. We project a first test of the DART chamber in the ArDM clone cryostat at CERN and a later installation in the ArDM setup at LSC.

Summary

2017 was an important year in the ArDM programme since a major milestone was reached, the operation of a tonne-scale LAr TPC in the dual-phase operational mode. Objectives of Run II for the project include a general assessment of the sensitivity of the setup for low energy nuclear recoils, the study of multiple-scatter neutron events, the improved electron-recoil rejection power (based on PSD and the S1/S2 ratio), as well as the study of related technical challenges, like the LAR VUV attenuation length in effect of the performance of a given purification system. All of these items are regarded to represent fundamental milestones towards large LAr Dark Matter detectors of the next generation. A mid-term programme for depleted argon tests with ArDM at LSC beyond these activities was identified and is well under preparation.

References

[1] ArDM Collaboration, J. Calvo et al., "Commissioning of the ArDM experiment at the Canfranc underground laboratory: first steps towards a tonne-scale liquid argon time projection chamber for Dark Matter searches," Journal of Cosmology and Astroparticle Physics 2017 (2017) 003, arXiv:1612.06375 [physics.ins-det]

[2] ArDM Collaboration, J. Calvo et al., "Measurement of the attenuation length of argon scintillation light in the ArDM LAr TPC," Astroparticle Physics 97,186 (2018), arXiv:1611.02481 [astro-ph.IM]

[3] ArDM Collaboration, J. Calvo et al., "Low energy backgrounds and pulse shape discrimination in the ArDM liquid argon TPC", arXiv:1712.01932 [physics.ins-det]

[4] Bárbara-Rosario Montes Núñez, "Analysis of the first underground run and background studies of the Argon Dark Matter experiment," PhD thesis, Complutense University of Madrid / CIEMAT, 2016.

[5] M. Battaglieri et al., "US Cosmic Visions: New Ideas in Dark Matter 2017: Community Report", arXiv:1707.04591v1 [hep-ph]

7 NEXT
NEXT-WHITE RESULTS DURING RUN II

http://next.ific.uv.es/next

1 Introduction

The NEXT program is developing the technology of high-pressure xenon gas Time Projection Chambers (TPCs) with electroluminescent amplification (HPXe-EL) for neutrinoless double beta decay searches [1–5]. The first phase of the program included the construction, commissioning and operation of two prototypes, called NEXT-DEMO and NEXT-DBDM, which demonstrated the robustness of the technology, its excellent energy resolution and its unique topological signal [6–9].

The NEXT-White[1] (NEW) detector implements the second phase of the program. NEXT-White is a ~ 1:2 scale model of NEXT-100 (the TPC has a length of 664.5 mm and a diameter of 522 mm while the NEXT-100 TPC has a length of 1300 mm and a diameter of 1050 mm), a 100 kg HPXe-EL detector, which constitutes the third phase of the program and is foreseen to start operations in

2019. NEXT-White has been running successfully since October 2016 at Laboratorio Subterráneo de Canfranc (LSC). Its purpose is to validate the HPXe-EL technology in a large-scale radiopure detector. This validation is composed of three main tasks: to assess the robustness and reliability of the technological solutions; to compare in detail the background model with data, particularly the contribution to the radioactive budget of the different components, and to study the energy resolution and the background rejection power of the topological signature characteristic of a HPXe-EL. Furthermore, NEXT-White can provide a measurement of the two-neutrino double beta decay mode ($\beta\beta 2\nu$).

During 2017 the NEXT collaboration has focused its effort in the operation and data analysis of the NEXT-White detector. This report presents a summary of the most important results obtained during that period. For a detailed discussion we refer to [10–14]. Other important results obtained during 2017 are found int [15–18].

2 The NEXT-White detectors: an overview

Table 1: NEXT-White TPC parameters.

TPC parameter	Nominal	Run II(4734)	Run II(4841)
Pressure	15 bar	7.2 bar	9.1 bar
EL field (E/P)	2.2 kV cm^{-1} bar^{-1}	1.7 kV cm^{-1} bar^{-1}	1.7 kV cm^{-1} bar^{-1}
EL gap V_{gate}	6 mm	6 mm	6 mm
Length	16.2 kV	7.0 kV	8.5 kV
Diameter	664.5 mm	664.5 mm	664.5 mm
Fiducial mass	454 mm	454 mm	454 mm
Drift length	5 kg	2.3 kg	3 kg
Drift field	(530.3 ± 2.0) mm	(530.3 ± 2.0) mm	(530.3 ± 2.0) mm
$V_{cathode}$	400 V cm^{-1}	400 V cm^{-1}	400 V cm^{-1}
	41 kV	28 kV	30 kV

The NEXT-White apparatus is currently the world's largest radiopure HPXe-EL. Table 1 shows the main parameters of the TPC. The left column lists the nominal (design) parameters, while the center and right columns list the operational parameters during the initial operation of the detector (the so-called Run II described later in this paper). The energy plane is instrumented with 12 Hamamatsu R11410-10 PMTs located 130 mm behind the cathode, providing a coverage of 31%.

1 Named after Prof. James White, our late mentor and friend.

The tracking plane is instrumented with 1792 SiPMs SensL series-C distributed at a pitch of 10 mm. An ultra-pure copper shell (ICS) 60 mm thick, acts as a shield in the barrel region. The tracking plane and the energy plane are supported also by pure copper plates 120 mm thick.

The detector operates inside a pressure vessel fabricated with a radiopure titanium alloy, 316Ti. The pressure vessel sits on a seismic table and is surrounded by a lead shield (the lead castle). Since a long electron lifetime is a must, the xenon circulates in a gas system where it is continuously purified. The whole setup sits on top of a tramex platform elevated over the ground at Hall-A, in the Laboratorio Subterráneo de Canfranc (LSC) (Figure 7.1).

Figure 7.1: *Top panel: a diagram showing the NEW detector and associated infrastructures at the LSC (the yellow beams mark the coverage of webcams for remote parameter control); bottom panel: a picture of the setup at the LSC.*

3 Krypton calibrations

In this section we describe the calibration of the detector using a rubidium source (83Rb) which provides a large sample of krypton (83mKr) decays, yielding a homogenous sample of 41.5 keV energy deposits. These point-like, evenly-distributed events permit to measure, correct for, and continuously monitor the drift-electron lifetime, as well as to measure and correct for the dependence of the measured energy on the transverse (x, y) coordinates. After correcting both effects, the energy resolution of the chamber for point-like energy deposits can be determined.

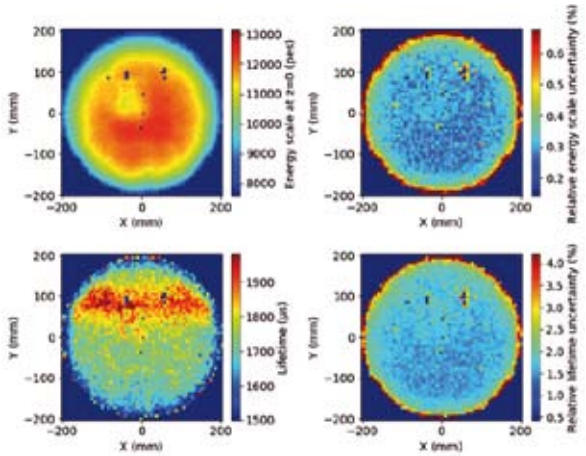

Figure 7.2: *Maps obtained by fitting the lifetime as a function of (x, y) for run 4734. The predicted energies for z = 0 (left) and their uncertainties (right) are displayed in the top row, while the lifetimes (left panel) and their uncertainties (right panel) are shown in the bottom row. A clear dependence of the lifetime on (x, y) is observed. The uncertainty in the energy scale is of the order of 0.2 %, making a sub-dominant contribution to the energy resolution at 41.5 keV. On the other hand, the uncertainty in the lifetime value is of the order of the 1% and cannot be neglected for the interpretation of the final value of the energy resolution.*

This dependence of the lifetime can be corrected using large-statistics krypton runs to produce a lifetime map.

The map is built by dividing the chamber in 60 × 60 bins, each bin being a 6.7 mm-size square and fitting for the lifetime in each bin. The number of bins is chosen to maximize

granularity while still keeping enough data in each bin so that the statistical uncertainties of the fits are small.

The resulting maps are shown in figure 2 for run 4734. The optimal parameters found by fitting the data correspond to the prediction of the energy at z = 0 and its uncertainty, as well as the lifetime and its uncertainty. Thus, the map displayed in the top-left panel is an energy map, where the effect of the lifetime has been factored out, showing the dependence of the event energy on (x, y). The map is rather uniform in the central region, with the exception of a "crater" centered around [−50, 50] whose origin we attribute to a few SiPM boards with degraded reflectance, and fall abruptly at large radius, as the solid angle covered by the PMTs falls to zero. The lifetime map is shown in the bottom-left panel. A region of larger lifetime (close to 2 ms) appears at large positive y, near the top of the chamber (the average lifetime in the center of the chamber is around 300 μs smaller).

The crucial point is that, while it is difficult to understand the complex physics that may lead to variable lifetime maps, krypton calibrations permit a correction for those effects.

3.1 Energy Resolution

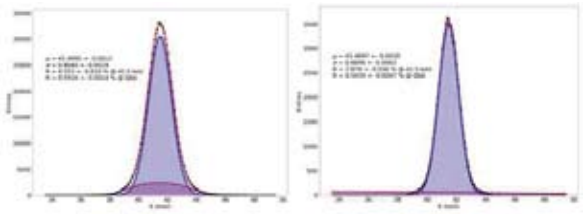

Figure 7.3: *Corrected energy distribution for krypton events (left) in the full volume of the NEXT- White TPC, and in a restricted fiducial volume (right), for run 4734. See text for details.*

To estimate the energy resolution for point like energy deposits in NEXT-White, the krypton data are divided in two samples. The correction (C) sample is used to compute the lifetime and geometry correction maps, which are then applied to the data in the measurement (M) sample. The corrected energy of the PMT sum is then fitted to a gaussian to estimate the energy resolution.

Figure 3 illustrates the energy resolution measured with run 4734 (at a pressure of 7.2 bar). The data are fitted to a double-gaussian, to take into account tails due to residual background events (small energy deposits or ^{83m}Kr decays with wrong S1 identification). The fit yields an energy resolution of (4.55 ± 0.01) % FWHM in the full NEXT-White volume (left panel). A naive 1/ √E extrapolation to $Q_{\beta\beta}$ yields (0.592 ± 0.001) %. The fit in the right panel corresponds to the data contained in a fiducial region defined by a radius smaller than 150 mm and z smaller than 150 mm. The radial cut ensures optimal geometrical coverage and the z cut minimizes the residual errors due to lifetime fluctuations, which increase with z. The fit yields (3.88 ± 0.04) %, extrapolating to (0.504 ± 0.005) % at $Q_{\beta\beta}$. This value is reasonably close to the best resolution expected in NEXT- White (figure 3), confirming the excellent capabilities of the technology and the good working conditions of the chamber. Figure 3 illustrates the energy resolution measured with run 4841 (at a pressure of 9.1 bar). The data are fitted to a gaussian plus a polynomial, to take into account tails due to residual background events (small energy deposits or ^{83m}Kr decays with wrong S1 identification). The fit yields an energy resolution of (4.53 ± 0.02) % FWHM in the full NEXT-White volume (left panel). A naive1/ √E extrapolation to $Q_{\beta\beta}$ yields (0.589 ± 0.002) %. The fit in the right panel corresponds to the data contained in the

fiducial region defined above. The fit yields (3.90 ± 0.03) %, extrapolating to (0.507 ± 0.003) % at $Q_{\beta\beta}$, similar to the values obtained for run 4734, and confirming that resolution for point-like energy deposits scales well with pressure.

The main systematic uncertainties in the energy resolution come from the uncertainties in the correction factors and the lifetime. We have estimated these uncertainties by measuring the variation in the energy resolution when those quantities are shifted ±1σ around the optimal value. We find for both runs that the contribution is 0.04% at 41.5 keV. Taken this into account, we get a final estimate of the energy resolution in the full volume of (4.55 ± 0.04) % ((0.592 ± 0.005) % at $Q_{\beta\beta}$) for the 7.2 bar run and (4.53 ± 0.04) % ((0.589 ± 0.005) % at $Q_{\beta\beta}$) for the 9.1 bar run.

4 Measurement of radon-induced backgrounds in the NEXT double beta decay experiment

Radon (^{220}Rn and particularly ^{222}Rn) has proven to be a serious concern for underground experiments searching for rare events, such as neutrinoless double beta decay (ββ0ν), dark matter interactions, or solar neutrino interactions. The β and γ particles produced in the β decays of ^{222}Rn progeny are potential backgrounds to these searches. In particular, the interactions of the high-energy (up to 3.3 MeV) γ particles produced in ^{214}Bi β decays can be a significant background in ββ0νexperiments. For this reason, all ββ0νexperiments require monitoring and mitigation of radon content. A schematic of the lower part of the naturally-occurring uranium (^{238}U) decay chain, starting from ^{222}Rn and ending in the long-lived ^{210}Pb isotope, is shown in Fig. 4. Similarly, ^{220}Rn is part of the thorium (^{232}Th) decay chain, which also includes several β decays of relevance for rare event searches. Air-borne radon is present in the atmosphere surrounding the detector. Internal radon can also be present within the detector volume, either via emanation from detector materials, or through air leaks from the surroundings.

The sensitivity of NEXT-100 to ^{136}Xe ββ0ν decay has been evaluated in [5], relying on detailed radio-assay measurements [16,33,34] and Monte-Carlo simulations. A background rate of 4 × 10−4counts/(keV kg y) at most is expected in the ββ0ν energy region of interest after all cuts, yielding a sensitivity of 6 × 10^{25} yr after an exposure of 275 kg·yr.

This sensitivity study assumed a negligible contribution from radon-induced backgrounds. The purpose of this work is to test this assumption. In particular, we focus here on internal radon within the xenon recirculation loop of NEXT, as air-borne radon is expected to be very effectively mitigated in the experiment.

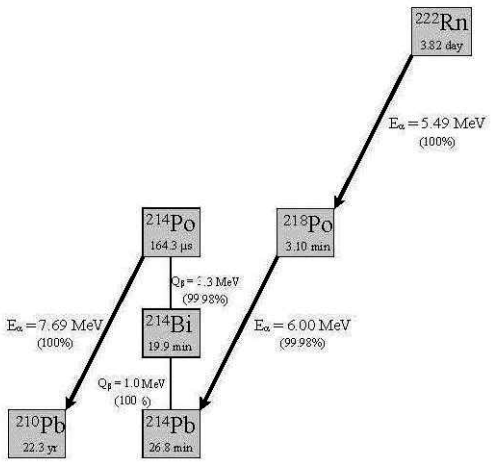

Figure 7.4: *Part of the 222Rn decay scheme that is most relevant for rare event searches.*

4.1 Radon-induced alpha particles

Three alpha run periods are considered. The first period (A1) corresponds to a time when the ambient temperature getter had not yet been turned on. This is the period used to estimate the ^{222}Rn internal activity for the upcoming physics runs in NEXT-White and NEXT-100. The second period (A2) was taken shortly after the ambient temperature getter was operated for the first time, during April 11 – 21, 2017. A number of short runs were taken over two weeks, to measure electron lifetime and to monitor how the high radon activity induced by the getter would decrease over time. The third period (A3) occurred shortly after a second period of operations with the ambient temperature getter (May 18 – July 12, 2017), again generating a high alpha production rate. The A3 sample is used to relate the ^{222}Rn-induced alpha production rate within the xenon fiducial volume with the rate of electrons from ^{214}Bi daughter plate-out on the cathode.

Figure 6 shows the time evolution of the inclusive alpha production rate during A2. DAQ dead-time effects are relevant, considering that the trigger rate was in the several Hz range and a trigger mask was set to 15 Hz during these runs. A 15 Hz trigger mask means that the DAQ cannot acquire additional events during a 1/15 s = 66.7 ms time period following a trigger. Given the known average trigger for each run, one can therefore estimate the DAQ efficiency as follows:

$$\varepsilon DAQ = 1 - R_{trg}/R_{max}$$

where R_{trg} is the average trigger rate measured, and R_{max} is the trigger mask. The inclusive alpha production rate both with and without the DAQ efficiency correction of Eq. 4.1 is shown in Fig. 7.4. The DAQ efficiency correction greatly improves the quality of the exponential fit, also shown in the figure. The exponential half-life returned by the fit over the entire A2 period is T1/2 = (3.822 ± 0.013) d. This value is in excellent agreement with the 222Rn half-life reported in the literature, $T_{1/2}$ (^{222}Rn) = (3.8235 ± 0.0003) d [35], confirming that alpha particles are induced by ^{222}Rn decays.

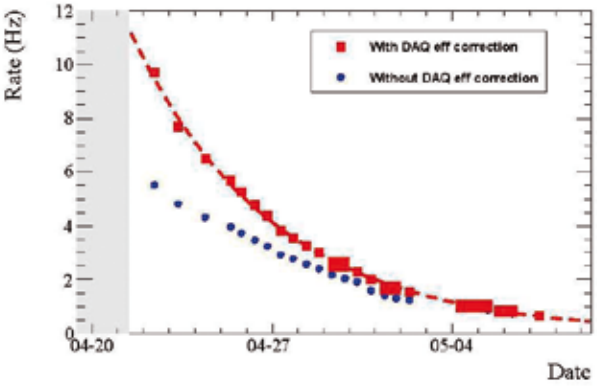

Figure 7.5: *Radon decay evolution during period A2, with and without DAQ efficiency correction. An exponential fit is superimposed.*

4.2 Radon activity measurement

The time evolution of the alpha production rate during the A2 period unambiguously identifies those particles as being induced from the decay of ^{222}Rn and its progeny. However, this information is not sufficient to disentangle the relative contributions of the ^{222}Rn (5489 keV), ^{218}Po (6002 keV) and ^{214}Po (7687 keV) alpha emitters in the chain, see Tab. 10, and hence to provide an absolute radon activity measurement. In addition, other alpha emitters might be present, for example from the decay of ^{222}Rn and its daughters. Because of these reasons, a spectroscopic analysis has been performed, with the goal of identifying the alpha-emitting isotopes. In order to reconstruct the alpha kinetic energy more reliably, a fiducial alpha candidate sub-sample within the inclusive sample has been

defined. This selection is illustrated in Fig. 6 by the solid black lines. The fiducial volume is defined to be 20 < Z < 520 mm and R < 178 mm. About 54% of the alpha candidates pass the fiducial requirement.

The alpha energy spectrum obtained during the high (A3) and low (A1) radon activity periods is shown in Fig. 12. For both periods, the ^{222}Rn and ^{218}Po populations are described by gaussian distributions. For A3, an excess of events compatible with ^{214}Po (7687 keV) is also visible and fitted with a third gaussian. For the lower statistics A1 period, no ^{214}Po contribution is visible. Only the overall normalizations of the alpha-emitting isotopes, plus the peak position and width of the ^{222}Rn population, are kept free in the fit. The peak position and width of the ^{218}Po and ^{214}Po populations are rescaled from the corresponding fit parameters of the 222Rn population, taking into account the known alpha kinetic energies.

For the high radon period A3, the fitted ^{222}Rn, ^{218}Po and ^{214}Po yields represent a (75.5 ± 0.3) %, (24.1 ± 0.2)% and (0.041 ± 0.008)% fraction of the observed fiducial alpha events, respectively.

The sum of the fitted yields are therefore compatible with 100%. For the low radon period A1, the fitted ^{222}Rn and ^{218}Po yields represent a (61.0 ± 3.7) % and (21.1 ± 2.9) % fraction of the observed fiducial alpha events, respectively. In the latter case, about a 18% fraction of observed alpha events is unaccounted for by the fit model. A specific 222Rn activity of (37.5 ± 2.3) mBq/m3 within the detector fiducial volume is obtained during A1. The 222Rn specific activity increases by three orders of magnitude during A3, taken only six days after closing the 222Rn-emanating ambient temperature getter.

4.3 Implications for double beta decay searches

Finally, we study the impact that radon-induced backgrounds are expected to have on the NEXT physics program. In the following, the implications for the two-neutrino double beta decay ($\beta\beta 2\nu$) measurement of ^{136}Xe in NEXT-White and for the neutrinoless double beta decay ($\beta\beta 0\nu$) search in NEXT-100 are discussed.

For NEXT-White, ^{214}Bi decays from the cathode have been simulated at 15 bar pressure, in anticipation of the operating pressure for the upcoming NEXT physics runs with ^{136}Xe-enriched xenon. Only simulated events with

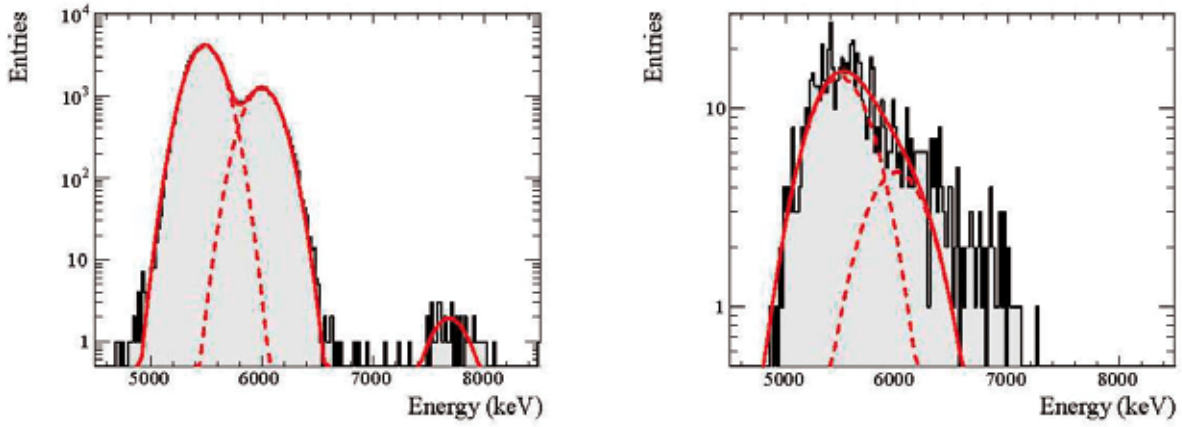

Figure 7.6: *Energy distribution for fiducial alpha candidate events during run periods A3 (left panel) and A1 (right panel). A triple gaussian fit is superimposed to the A3 histogram to describe the 222Rn (5489 keV), 218Po ((6002 keV) and 214Po (7687 keV) populations. Only the 222Rn and 218Po yields are fitted in the A1 histogram.*

a minimum deposited energy of 600 keV are kept for further processing. A fully realistic simulation has been performed. Energy and hit reconstruction for simulated data are obtained by using the same algorithms that are applied to real data.

The left panel of Fig. 7.7 shows the reconstructed energy for NEXT-White ^{214}Bi events simulated from the cathode, and passing all ββ2ν cuts in Table 2. Unit-area normalized distributions for both the full and fast analyses are shown. The agreement between the fast and full analysis energy distribution shapes is excellent. A number of full energy deposition gamma-ray lines are clearly visible, at 768, 1120 and 1764 keV energies. In addition, the double-escape peaks at 1182 and 1426 keV from the 2204 and 2448 keV gamma-ray lines, respectively, are also visible.

From the 222Rn specific activity measurement during the low-radon alpha run, (37.5±6.3) mBq/m3 as discussed in Sec. 4.2, the radon-induced background rate for the upcoming ββ2ν measurement in NEXT-White has been estimated. We assume ^{222}Rn concentration to be uniform throughout the full active (530.3 mm long) and buffer (130 mm long) volumes, with radius 198 mm. The total ^{222}Rn activity is therefore (3.06 ± 0.51) mBq. The same activity is assumed for ^{214}Bi decays from the cathode. For a 6.2 × 10−4 background acceptance after cuts as obtained from the full ββ2ν analysis in Table 2, a total radon-induced background rate of (60 ± 10) counts/yr is obtained. This rate is more than three orders of magnitude smaller than the background expected from ^{60}Co, ^{40}K, ^{214}Bi and ^{208}Tl decays altogether from radioactive impurities trapped in the NEXT-White detector components. Radon-induced backgrounds will therefore be negligible in NEXT-White.

Simulations have also been performed for cathode ^{214}Bi decays in NEXT-100. The simulation, reconstruction and analysis steps follow the ones described above for NEXT-White, with two exceptions. First, only a fast ββ0ν analysis as in [5] has been performed in this case, since the tools to perform a full analysis in NEXT-100 are still under development. Second, the event selection is optimized for the ββ0ν search. As such, a minimum deposited energy per event of 2300 keV is required for further processing, and the energy ROI is defined to be $2453 < E_{reco} < 2475$ keV. All other reconstruction and selection steps are identical to the ones described above, including the fiducial requirement of no reconstructed hits within 20 mm of the detector active volume boundaries. Table 2 gives also the event reduction summary

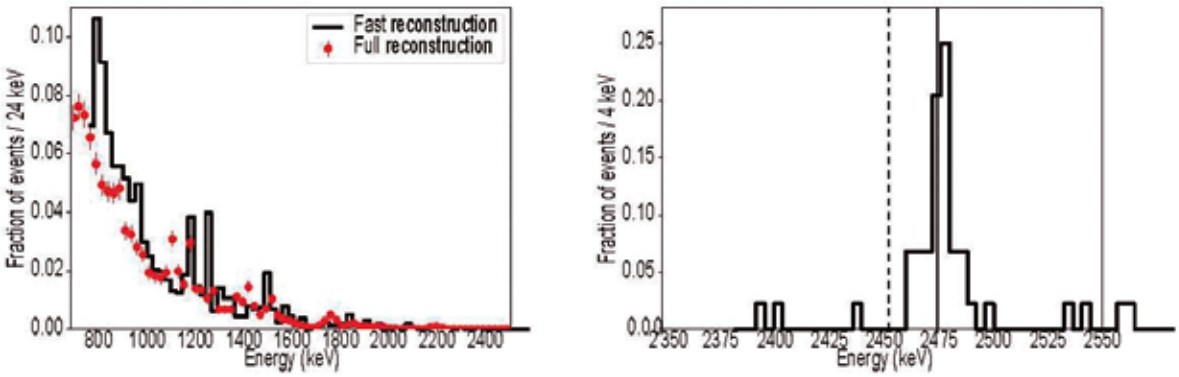

Figure 7.7: *Distributions of reconstructed event energy for cathode 214Bi simulated decays. Left panel: simulated events in NEXT-White at 15 bar and passing all ββ2νcuts. The black histograms show the expectations from the fast analysis, the red markers from the full analysis. Right panel: simulated events in NEXT-100 at 15 bar and passing all ββ0νfast analysis cuts except the energy ROI one, indicated by the vertical dashed lines. All curves are unit-area normalized.*

of NEXT-100 ^{214}Bi background events from the cathode and for the fast ββ0ν analysis. Primarily because of the stricter energy requirement, a much smaller background acceptance is obtained, 7×10^{-8}. We can also use Table 2 to approximately estimate the cathode ^{214}Bi background rejection in NEXT-100 if a full ββ0ν analysis were available. To this end, we multiply the 7×10^{-8} background acceptance figure by the ratio of the NEXT-White full and fast analysis acceptances, to obtain an acceptance of about 2.7×10^{-7}.

The right panel of Fig. 7 shows the unit-area normalized energy distribution for ^{214}Bi cathode events in NEXT-100 passing all ββ0ν cuts except the energy ROI one. The distribution is dominated by the 2448 keV gamma-ray line of ^{214}Bi, located only 10 keV below the ^{136}Xe Qββ value. Events in the high-energy tail of the 2448 keV reconstructed energy peak can pass the energy ROI selection, also shown in the figure with vertical lines.

Scenario	Total ^{214}Bi activity from cathode (counts/yr)	Background acceptance	ββ0νbackground rate (counts/yr)
Optimistic	$(9.7 \pm \pm 1.6) \times 10^4$	7×10^{-8}	$(6.8 \pm 1.1) \times 10^{-3}$
Pessimistic	$(6.0 \pm \pm 1.0) \times 10^5$	2.7×10^{-7}	0.16 ± 0.03

Table 2: *Radon-induced background rates expected in NEXT-100 under different assumptions. The background acceptances and background rates refer to the ββ0νselection.*

Table 2 shows the radon-induced background rate expected in NEXT-100 ββ0ν searches, again starting from the NEXT-White radon activity measurement in Sec. 4.2, and the background acceptance numbers quoted above. The background prediction is more uncertain in this case, for two reasons. First, as we have not identified the radon source in the NEXT-White measurement, some uncertainty exists on how the total ^{222}Rn activity extrapolates from NEXT-White to NEXT-100. In the optimistic scenario, radon emanation is dominated by gas system components external to the detector vessels. As the same gas system is foreseen for NEXT-White and NEXT-100 operations, in this case the total ^{214}Bi activity from the cathode would be the same in both detectors. In the pessimistic scenario, radon emanation is dominated by inner detector components, and the radon total content would scale with detector surface area, about 6 times larger in NEXT-100 compared to NEXT-White. Second, the lack of full analysis results in NEXT-100 introduces an additional uncertainty arising from the background rejection performance for this event topology. For the pessimistic scenario, we take the 2.7×10^{-7} background acceptance number given above. For the optimistic scenario, we assume 7×10^{-8}. Despite the fact the latter number is not based on a full simulation and reconstruction, we consider it to be a realistic estimate of the best possible background rejection performance, as more detailed simulations in the future will be accompanied by improvements in event reconstruction and selection.

As a result, we define two extreme scenarios in Tab. 2. The optimistic one assumes the lowest possible radon content in the detector, and the best possible background rejection. A radon-induced background rate of only $(6.8 \pm 1.1) \times 10^{-3}$ counts/yr is expected in this case. The pessimistic scenario assumes high radon content, and the worst background rejection number. The background rate is expected to be 0.16 ± 0.03 counts/yr in the pessimistic scenario. These numbers should be compared with the background rate expected from radioactive impurities in detector materials, estimated to be at the level of 4×10^{-4} counts/(keV·kg·yr), or 0.7 counts/yr [5]. Hence, the NEXT-White measurement allows us to constrain the radon-induced background to be at most of the same order as the detector radioactive impurities, and possibly much smaller. In any case, we can

conclude that radon-induced backgrounds will remain at a tolerable level for the NEXT-100 physics program. A campaign to quantify radon emanation from NEXT detector and gas system components is underway, to identify the dominant radon sources and hence to further reduce the uncertainties in the extrapolation from the NEXT-White measurement to NEXT-100.

5 Demonstration of Single Barium Ion Sensitivity for Neutrinoless Double Beta De- cay using Single Molecule Fluorescence Imaging

Single molecule fluorescence imaging (SMFI) is a technique invented by physicists and developed by biochemists that enables single-molecule sensitive, super-resolution microscopy. Among the applications of SMFI are the sensing of individual ions [36], demonstrated in various environments, including inside living cells [37]. A fluor is employed that is non-fluorescent in isolation, but becomes fluorescent upon chelation with a suitable ion. The molecule typically comprises of a dye bonded to a receptor that traps the ion in a cage-like structure. The electrostatic forces exhibited by the ion on the dye modify its energy levels to enable molecular fluorescence. Detection is assisted by the inherent stokes shift of the dye, allowing separation of emission and excitation light via dichroic filters. Localized light emission from single molecules can be spatially resolved using electron multiplying CCD (EM-CCD) cameras, allowing rejection of backgrounds from scattering and low-level fluorescence of unchelated molecules, which are diffuse.

The NEXT collaboration is pursuing a program of R&D to employ SMFI techniques to detect the barium daughter ion in high pressure xenon gas (HPGXe).

To demonstrate single Ba++ sensitivity we have imaged individual near-surface Ba++ ions from dilute barium salt solutions. We use the technique of through-objective total internal reflection fluorescence (TIRF) microscopy [38].

The hallmark of single molecule fluorescence is a sudden discrete photo-bleaching transition [39]. This occurs when the fluorophore transitions from a fluorescent to a non-fluorescent state, usually via interaction with reactive oxygen species [40]. This discrete transition signifies the presence of a single fluor, rather than a site with multiple fluors contributing. The 375 s scan time is significantly longer than the typical photo-bleaching time of Fluo-3 at this laser power [40], so the majority of spots are observed to bleach in our samples. A typical near-surface fluorescence trajectory is shown in Fig. 7.8. One 0.5 s exposure of this spot directly before

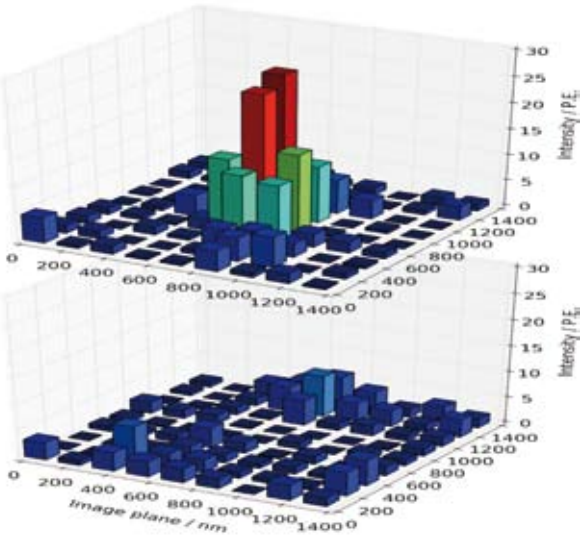

Figure 7.8: *A single Ba++ candidate. A fixed region of the CCD camera is shown with 0.5 s exposure before (top) and after (bottom) photo-bleaching transition.*

the step and one 0.5 s exposure directly after the step are also shown.

The barium-free and barium-spiked samples were analyzed over a total of 22 FOVs each. Across the barium-free samples, a total of 75 candidates were resolved passing all cuts. Across the barium-spiked samples, a total of 187 were resolved, representing a statistical excess of ~12.9 σ.

The actual signal-to-background ratio is larger than is suggested by this comparison, due to the FOV selection bias requiring at least one bright spot to be found in order to focus. The number of candidates per FOV is shown in Fig. 7.9. In this histogram, each entry is weighted by the number of candidates observed, such that the integral is equal to the total number of candidate ions identified.

The candidates in the barium-free samples are understood to derive from residual ion contamination in the Ultra Trace water. In a real barium tagging sensor this background is un-problematic, since the tagging signature is the arrival of a new ion in coincidence with a tagged event. The presence of persistent background fluorophores does not obscure this, unless there are so many that the image is saturated. The size of the FOV used here and the level of surface contamination suggests that at least 105 Ba++ ions will be detectable per sensor before saturation.

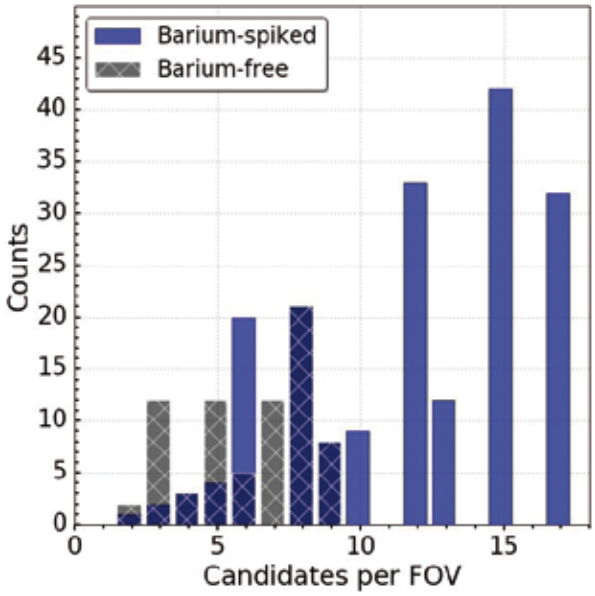

Figure 7.9: *Histogram showing number of ion candidates per FOV in barium-free and barium-spiked samples. Entries are weighted by candidates detected.*

6 Summary

This report summarizes the progress made by the NEXT collaboration during 2017 concerning the data analysis of acquired with the NEXT-White detector during Run II. The results presented include: a measurement of the drift properties of electrons in NEXT-White a measurement of the energy resolution that can be obtained for point-like energy depositions (e.g, krypton decays), together with a procedure to calibrate the detector, providing maps to correct lifetime and geometrical effects; a measurement of alpha particles in NEXT-White, together with an exhaustive analysis of the expected impact of radon in NEXT-100. These last results are especially relevant for the future operation of the NEXT-100 detector. Last but not least, we present a demonstration of the feasibility of Ba++ tagging using SFMI.

Calibration data obtained with ^{137}Cs and Þ data is currently under analysis to determine a first estimation of the resolution that NEXT-White can attain for long tracks, as well as to demonstrate the separation between single and double electrons and results will be available shortly.

In summary, the initial operation of the NEXT-White detector shows promising results both in terms of detector performance and radon backgrounds.

Acknowledgments

The NEXT Collaboration acknowledges support from the following agencies and institutions: the European Research Council (ERC) under the Advanced Grant 339787-NEXT; the European UnionâAZs Framework Programme for Research and Innovation Horizon 2020 (2014-2020) under the Marie SkÅC´odowska-Curie Grant Agreements No. 674896, 690575 and 740055; the Ministerio de Economía y Competitividad of Spain under grants FIS2014-53371-C04, the Severo Ochoa Program SEV-2014-0398 and the María de Maetzu Program MDM-2016-0692; the GVA of Spain under grants PROMETEO/2016/120 and SEJI/2017/011; the Portuguese FCT and FEDER through the program COMPETE, projects PTDC/FIS-NUC/2525/2014 and UID/FIS/04559/2013; the U.S. Department of Energy under contracts number DE-AC02-07CH11359 (Fermi National Accelerator Laboratory), DE-FG02-13ER42020 (Texas A&M) and de-sc0017721 (University of Texas at Ar- lington); and the University of Texas at Arlington. We also warmly acknowledge the Laboratorio Nazionale di Gran Sasso (LNGS) and the Dark Side collaboration for their help with TPB coating of various parts of the NEXT-White TPC. Finally, we are grateful to the Laboratorio Subterráneo de Canfranc for hosting and supporting the NEXT experiment.

References

[1] David Nygren. High-pressure xenon gas electroluminescent TPC for 0 − ν ββ-decay search. *Nucl.Instrum.Meth.,* A603:337–348, 2009.

[2] V. Álvarez et al. The NEXT-100 experiment for neutrinoless double beta decay searches (Conceptual Design Report). 2011.

[3] V. Álvarez et al. NEXT-100 Technical Design Report (TDR): Executive Summary. *JINST* , 7:T06001, 2012.

[4] J. J. Gomez-Cadenas et al. Present status and future perspectives of the NEXT experiment. *Adv. High Energy Phys.,* 2014:907067, 2014.

[5] J. Martín-Albo et al. Sensitivity of NEXT-100 to Neutrinoless Double Beta Decay. *JHEP,* 05:159, 2016.

[6] V. Álvarez et al. Initial results of NEXT-DEMO, a large-scale prototype of the NEXT-100 experiment. *JINST* , 8:P04002, 2013.

[7] V. Alvarez et al. Operation and first results of the NEXT-DEMO prototype using a silicon photomultiplier tracking array. *JINST* , 8:P09011, 2013.

[8] V. Álvarez et al. Near-Intrinsic Energy Resolution for 30 to 662 keV Gamma Rays in a High Pressure Xenon Electroluminescent TPC. *Nucl. Instrum. Meth.,* A708:101–114, 2012.

[9] P. Ferrario et al. First proof of topological signature in the high pressure xenon gas TPC with electroluminescence amplification for the NEXT experiment. *JHEP,* 01:104, 2016.

[10] F. Monrabal et al. The Next White (NEW) detector. 2018.

[11] A. Simón et al. Electron drift properties in high pressure gaseous xenon. 2018.

[12] G. Martínez-Lema et al. Calibration of the NEXT-White detector using 83m Kr decays. 2018. [13] P. Novella et al. Measurement of radon-induced backgrounds in the NEXT double beta decay experiment. 2018.

[14] A. D. McDonald et al. Demonstration of Single Barium Ion Sensitivity for Neutrinoless Double Beta Decay using Single Molecule Fluorescence Imaging. *Phys. Rev. Lett.,* 120(13):132504, 2018.

[15] R. Felkai, F. Monrabal, Diego Gonzalez-Díaz, M. Sorel, N. López-March, et al. Helium-Xenon mixtures to improve topological signature in high pressure gas Xenon TPCs. 2017.

[16] S. Cebrián et al. Radiopurity assessment of the energy readout for the NEXT double beta decay experiment. *JINST* , 12(08):T08003, 2017.

[17] A. Simón et al. Application and performance of an ML-EM algorithm in NEXT. *JINST* , 12(08):P08009, 2017.

[18] C. A. O. Henriques et al. Secondary scintillation yield of xenon with sub-percent levels of CO2 additive for rare-event detection. *Phys. Lett.,* B773:663–671, 2017.

[19] B. Rebel et al. High Voltage in Noble Liquids for High Energy Physics. *JINST* , 9:T08004, 2014.

[20]V. Boccone et al. Development of wavelength shifter coated reflectors for the ArDM argon dark matter detector. *JINST* , 4:P06001, 2009.

[21] K. Lung, K. Arisaka, A. Bargetzi, P. Beltrame, A. Cahill, et al. Characterization of the Hamamatsu R11410-10 3-in. photomultiplier tube for liquid xenon dark matter direct detection experiments. *Nuclear Instruments and Methods in Physics Research A,* 696:32–39, December 2012.

[22] Sigma-aldrich. http://www.sigmaaldrich.com/catalog/product/aldrich/483095?lang=es&region=ES.

[23] A. Herzenberg. Attachment of slow electrons to oxygen molecules. The Journal of Chemical Physics, 51(11):4942–4950, 1969.

[24] M. Huk, P. Igo-Kemenes, and A. Wagner. Electron attachment to oxygen, water, and methanol, in various drift chamber gas mixtures. Nuclear Instruments and Methods in Physics Research Section A: Accelerators, Spectrometers, Detectors and Associated Equipment, 267(1):107 – 119, 1988.

[25] J. L. Pack, R. E. Voshall, and A. V. Phelps. Drift velocities of slow electrons in krypton, xenon, deuterium, carbon monoxide, carbon dioxide, water vapor, nitrous oxide, and ammonia. Phys. Rev., 127:2084–2089, Sep 1962.

[26] J. L. Pack, R. E. Voshall, A. V. Phelps, and L. E. Kline. Longitudinal electron diffusion coefficients in gases: Noble gases. Journal of Applied Physics, 71(11):5363–5371, 1992.

[27] S. R. Hunter, J. G. Carter, and L. G. Christophorou. Low-energy electron drift and scattering in krypton and xenon. Phys. Rev. A, 38:5539–5551, Dec 1988.

[28] T. Koizumi, E. E Shirakawa, and I. Ogawa. Momentum transfer cross sections for low-energy electrons in krypton and xenon from characteristic energies. Journal of Physics B: Atomic and Molecular Physics, 19(15):2331, 1986.

[29] V. Álvarez et al. Ionization and scintillation response of high-pressure xenon gas to alpha particles. JINST , 1305:P05025, 2013.

[30] D. Lorca et al. Characterisation of NEXT-DEMO using xenon Kα X-rays. JINST , 9(10):P10007, 2014. [31] H. Kusano, J. A. M. Lopes, M. Miyajima, and N. Hasebe. Longitudinal and transverse diffusion of electrons in high-pressure xenon. Journal of Instrumentation, 8(01):C01028, 2013.

[32] G. Martínez-Lema et al. Calibration of the NEXT-White detector using 83m Kr decays. JINST, in preparation.

[33] V. Álvarez et al. Radiopurity control in the NEXT-100 double beta decay experiment: procedures and initial measurements. JINST , 8:T01002, 2012.

[34] S. Cebrián et al. Radiopurity assessment of the tracking readout for the NEXT double beta decay experiment. JINST , 10(05):P05006, 2015.

[35] Sukhjeet Singh, A. K. Jain, and Jagdish K. Tuli. Nuclear Data Sheets for A = 222. Nucl. Data Sheets, 112:2851–2886, 2011.

[36] Yin Lu and Matthew F. Paige. An ensemble and single-molecule fluorescence spectroscopy investigation of calcium green 1, a calcium-ion sensor. Journal of Fluorescence, 17(6):739–748, Nov 2007.

[37] N Stuurman and RD Vale. Imaging single molecules using total internal reflection fluorescence microscopy, 2006.

[38] Thomas P Burghardt. Measuring incidence angle for through-the-objective total internal reflection fluorescence microscopy. Journal of Biomedical Optics, 17(12):126007, dec 2012.

[39] Satoshi Habuchi, Ryoko Ando, Peter Dedecker, Wendy Verheijen, Hideaki Mizuno, et al. Reversible single-molecule photoswitching in the gfp-like fluorescent protein dronpa. Proceedings of the National Academy of Sciences of the United States of America, 102(27):9511–9516, 2005.

[40] D Thomas, SC Tovey, TJ Collins, MD Bootman, MJ Berridge, et al. A comparison of fluorescent ca2+ indicator properties and their use in measuring elementary and global ca2+ signals. *Cell calcium,* 28(4):213–223, 2000.

8 BiPo
NEUTRINOLESS DOUBLE BETA DECAY: CANFRANC WITH MODANE
http://nemo.in2p3.fr/nemow3/

The BiPo-3 detector is a low-radioactivity detector dedicated to measuring ultra-low natural radionuclide contaminations of ^{208}Tl (^{232}Th chain) and ^{214}Bi(^{238}U chain) in thin materials.

The detector has been developed to measure the radiopurity of the double-beta decay source foils of the SuperNEMO experiment, since one of the main sources of background for SuperNEMO is a possible contamination of ^{208}Tl and ^{214}Bi produced inside the source foils.

The first module of SuperNEMO, called demonstrator, will contain 7 kg of ^{82}Se in the form of foils. The SuperNEMO foils are strips, 270 cm long, 13.5 cm wide and ~200 ~m thick.A total of 36 foils will accommodate the required mass. The first 11 foils have been produced with the same technique as in NEMO-3 by ITEP in Russia. However, the first measurements of these foils resulted in a ^{208}Tl activity about 20 µBq/kg, too high for the SuperNEMO requirements. Thus, a new technique for the source production has been developed by LAPP in France and a novel purification technique has been developed in JINR, Russia. During the year 2017 the BiPo-3 detector was dedicated to the measurement of the foils produced at LAPP. With this measurement, the screening of the SuperNemo foils has been finalized.

This report presents 1- the results of the measurements carried out during the year 2017 and 2- a summary of the radiopurity of the SuperNemo double beta source foils aforementioned as measured with BiPo-3.

1. Radiopurity of foils produced by chromatographic purification and new production protocol

A novel technique for selenium purification has been developed by JINR in Russia based on ion exchange chromatography.

The purified ^{82}Se powder is mixed with Polyvinyl alcohol (PVA) glue and then deposited between two Mylar sheets. We remind that the radiopurity of the Mylar and the PVA glue have been measured separately with the BiPo-3 detector.

The first SuperNemo foils have been produced using Mylar containing microscopic holes in order to ensure a good bonding. Radiopurity measurements showed that during the process of hole production, the Mylar was contaminated.

Therefore, the new production technique developed a new method to produce a stand-alone foil and uses Mylar without holes (raw Mylar) as an envelope to protect the foil.

Two measurements were carried out: 1) 15 Dec 2016 to 19 March 2017 and 2) 28 April 2017 to 7 August 2017. The results correspond to A(^{208}Tl) = 22 [8 - 54] µBq/kg at 90 % C.L. For the ^{214}Bi measurement, the analysis showed that the number of events in the data is compatible with the expected background fluctuation and allowed to set an upper limit to the contamination inside the ^{82}Se+PVA mixture of A(^{214}Bi) < 595 µBq/kg at 90 % C.L.

2. Summary of radiopurity results of the SuperNemo foils

Table I summarizes the results for the SuperNemo foils produced by the two methods mentioned above as measured with the BiPo-3 detector. It is worth noting that in spite of the difference in purification and production methods, the radiopurity levels of the foils are comparable (within statistics).

Foils	Mass ^{82}Se (kg)	Purification	Production	A(^{208}Tl) μBq/kg	A(^{214}Bi) μBq/kg
1	1.95	Double distillation	ITEP (Russia) With Mylar with holes	20 [11 – 32]	< 290 290 ± 290
2	1.5	Inverse chromatography	LAPP (France) With raw Mylar	22 [8 – 54]	< 595

Table 1: *Radiopurity results for two types of double-beta source foils to be installed in the SuperNemo demonstrator. . The 82Se mass refers to the total mass in the demonstrator.*

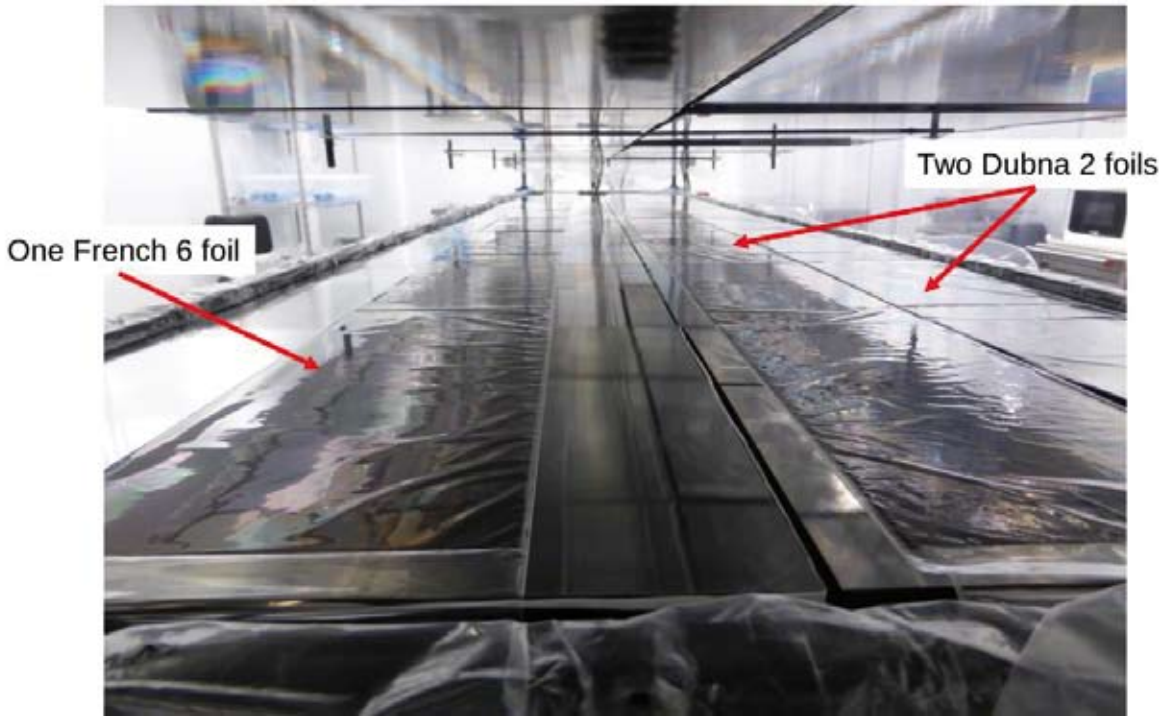

Fig 8.1: *SuperNemo double beta foils installed in BiPo-3.*

9 SuperKGd

SEARCHING FOR RADIO-PURITY: CANFRANC WITH KAMIOKA

http://www-sk.icrr.u-tokyo.ac.jp/sk/index-e.html

The SuperKGd-lsc project consist of a full series of radio-purity measurements and studies that we are carrying out at the LSC for the upgrade of the Super-Kamiokande experiment (SuperK-Gd) at the Kamioka Observatory (ICRR, U. Tokyo, Japan), by dissolving a Gadolinium (Gd) salt in its water.

Key in the project is the Gd salt since it will be present along the whole active fiducially volume of Super-Kamiokande, more than 25000 tons of water (total volume 50000 tons). During the previous years we could establish an extremely fruitful collaboration with four producers of Gd salts; among them we are almost decided which one is our best candidate for the mass production of the final Gd-salt. The four companies are the three Japanese *Nippon Yttrium Co. Ltd., Shinetsu Chemicals and Kanto Chemicals,* and the North America's *Molycorp Inc. (also Neo Performance Materials)*. In order to keep the confidentiality necessary at this stage of the Program, we will refer those as companies-*A, B, C and D.* Notice that the ordering is different.

The measurements by **SuperKGd-lsc** keep increasing their precisions, in particular to cope with the nowadays very high purities of some of the salts.

The instruments used up to know are the High Purity Ge Detectors of the LSC radio-purity service. Starting from sometime next year 2018, those particular very long-lived radioactive isotopes will be also measured with an even better precision by the new Inductively Coupled Plasma Mass Spectrometry system, ICP-MS, now under commissioning in the LSC. On the other side, in the Kamioka Observatory the preparations for the first phase of the project, the refurbishment of the Super-Kamiokande tank, are well under schedule.

The start is on June 1st 2018, when the tank will be opened, the water draining will start, and an "army" of technicians and scientists will go inside for the different jobs to be carried out that will last until approximately middle of October 2018.

The results by **SuperKGd-lsc** along their impact on the main Gd project of Super-Kamiokande have been presented at major conferences and workshops in the field. Those presentations by members of the **SuperKGd-lsc** team are:

- *SuperK-Gd; Luis Labarga at ``The Conference of the European Physical Society on High Energy Physics" (EPS-HEP 2017) '', Venice (Italy), July 2017*

Two doctoral thesis, with their doctoral job being crucial parts of **SuperKGd-lsc,** have been defended during 2017:

- *Neutrino Physics In Present And Future Kamioka Water-Cherenkov Detectors With Neutron Tagging; Pablo Fernandez Menendez, PhD. Thesis; UAM, March 2017*
- *Radioactive Contamination in Neutrino Experimental Physics: the Cases of NEXT and Super-Kamiokande Experiments; Javier Perez, PhD. Thesis; UAM, September 2017*

Chain	Main subchain Isotope	Gd2O3_ 201510-D Measured: 201510	GSF-1701-D-003	GSF-1705-D-001	GSF-1711-D-171111B	GSF-1711-D-171111A
^{238}U	^{238}U	1672 ± 122	< 45	< 11	< 52	< 168
	^{226}Ra	< 2.8	0.4 ± 0.2	4.3 ± 0.6	< 1.1	2.0 ± 1.4
^{232}Th	^{228}Ra	259 ± 6	28.5 ± 1.1	12.2 ± 1.0	300 ± 7	778 ± 39
	^{228}Th	124 ± 3	6.3 ± 0.5	2.5 ± 0.4	31 ± 2	70 ± 3
^{235}U	^{235}U	28.7 ± 1.5	< 1.5	< 1.0	< 3	< 4
	^{227}Ac/^{227}Th	< 14	< 5.5	3.4 ± 1.4	31 ± 5	46 ± 9
	^{40}K	21 ± 6	< 1.0	< 1.8	27 ± 3	57 ± 4
	^{138}La	< 3.2	< 0.25	< 0.36	< 2.4	< 2.4
	^{176}Lu	5.9 ± 0.4	26.5 ± 0.8	6.1 ± 0.4	< 1.2	4.3 ± 0.6

Table 1: *summary of measurement results of Gd salts from Company-D. See text for details. Units are mBq/Kg; limits are at 95% C.L. The 2017 measurements are in the four right columns.*

Activities. The radio-purity measurements on samples of Gd salts carried out during the year 2017 are listed below, along with some explanation to put them in context.

1, 2, 3, 4; One sample of $Gd_2(SO_4)_3$ from a new production iteration by *company-D* [GSF-1701-D-003] with the detector Asterix. There is a dramatic improvement in RI cleanness with respect to the first sample provided by company-D time ago. Table 1. These were good news since, given the lack of progress, it appeared to us that *company-D* had reduced significantly its interest in our Project. On the contrary, a new sample by company-D was delivered and shipped to Canfranc for measurement right after it (see next paragraphs). One sample of approx. 5 Kg of $Gd_2(SO_4)_3$ from a newer production iteration by company-D [GSF-1705-D-001] with the detector *Obelix*. It showed an improvement of an almost factor 2 in the ^{232}Th chain with respect to the previous one. However the lower part of the ^{238}U chain (^{226}Ra downwards) was somehow deteriorated. Two later samples, approx. 5 Kg of $Gd_2(SO_4)_3$ each, from two new production iterations by the same *company-D*. [GSF-1711-D-171111A, GSF-1711-D-171111B] with the detector *geTobazo*. Despite of the very

Chain	Main subchai Isotope	GSF-1703-A-702142	GSF-1703 B- (RGD-OSF-005)
^{238}U	^{238}U	< 13	< 13
	^{226}Ra	0.7 ± 0.4	< 0.34
^{232}Th	^{228}Ra	< 0.39	< 0.39
	^{228}Th	1.7 ± 0.4	< 0.28
^{235}U	^{235}U	< 1.3	< 0.77
	^{227}Ac/^{227}Th	< 3.1	< 2.3
	^{40}K	< 8.2	< 3.2
	^{138}La	< 0.29	< 0.29
	^{176}Lu	2.6 ± 0.3	< 0.29

Table 2: *summary of measurement results for the samples of Gd salts by company-A (left) and company-B (right). Units are mBq/Kg; limits are at 95% C.L.*

promising improvement that was obtained in the previous sample [GSF-1705-D-001], the new ones show much larger contaminations, unacceptable by several orders of magnitude, particularly for the ^{232}Th. Table 1. This was relevant information that was transmitted to *company-D* for any possible correction.

5; One sample of $Gd_2(SO_4)_3$ from *company-A* [GSF-1703-A-702142] with the detector Obelix. Up to now all the samples provided by *company-A* were small and produced at the company's laboratories, and all the information on radioactive-isotope was provided by the Company itself, from ICP-MS measurements. They featured excellent cleanness of isotopes ^{238}U and ^{232}Th. This was the first sample produced at Factory (regular production process) and, also, it was the first sample measured by Ge detectors, thus accessing to the whole radioactive chains and also to other isotopes with intermediate life times. In fact our measurements confirmed the lack of ^{238}U and ^{232}Th isotopes but they showed instead small but significant contaminations from the lower parts of the chains. This was relevant information that was transmitted to *company-A* for any possible correction.

6, 7, 8, 9; One sample of $Gd_2(SO_4)_3$ from a new production batch by *company-B* [GSF-1611-B-003] with the detector *Asterix*. This batch featured the use of a more radio pure H_2SO_4 at the last stage of production in an attempt to further reduce the already excellent purity achieved in [GSF-1604-B-001]. This sample became the cleanest of the whole **SuperK-Gd-lsc** project at that time (Table 3, along with previous samples from *company-B*).

A $Gd_2(SO_4)_3$ sample of a new "ultrapure-production" batch by company-B [GSF-1703-B-(RGD-OSF-005)], 3 Kg, detector *Asterix*. The results were excellent (Table 3).

On the other hand, profiting of a second sample of the same batch that was prepared for other purposes, we did perform a non-trivial check of stability/reproducibility of results. This sample was shipped following a rather different procedure and it traveled a path also different than the regular samples that we normally receive. In addition we did use a different detector for the measurement [GSF-1703-B- (RGD-OSF-005)-b], 3.4 Kg, detector *Obelix*. Both measurements are nicely consistent (Table 3) this supporting both, the correctness of our measurement protocols, and the uniformity of the quality within a single production batch.

Yet another sample of a new high purity production batch by company B as well [GSF-1707-B-007], 5 Kg, detector *Asterix*. This sample was the cleanest of the whole **SuperK-Gd-lsc** project so far (see results in Table 3, along with previous samples from *company-B*) … until the latest samples by *company-C* arrived.

10, 11, 12; Three samples, approximately 5 Kg. each, of $Gd_2(SO_4)_3$ from *company-C*. Each sample comes from each of the three production batches of the 500 Kg of Gd2(SO4)3 to dissolve in the 200 ton tank EGADS for its phase as Supernova detector. They are GSF-1710-C-170901, GSF-1710-C-170902 and GSF-1710-C-170903. The three measurements have been carried out with the detector *Asterix*. The results are excellent: the samples are within specs for the Uranium chains and cleaner than our measurement limits (which are already very good) for the Th chain. See Table 4. Basically *company-C* is ready for mass production.

Chaina	Main Sub-chain Isotope	GOX-1603-B-237	GOX-1603-B-239	GOX-1603-B-236	GSF-1604-B-1	GSF-1611-B-003	GSF-1703-B-(RGD-OSF-005)	GSF-1703-B-(RGD-OSF-005)-b	GSF-1707-B-007
^{238}U	^{238}U	< 68	< 130	< 36	< 25	< 13	< 10	< 19	< 10
	^{226}Ra	< 0.9	< 1.0	< 1.4	< 0.6	< 0.3	< 0.31	< 0.54	< 0.18
^{232}Th	^{228}Ra	< 2.7	< 2.3	< 1.4	< 0.7	< 0.3	< 0.30	< 0.74	< 0.21
	^{228}Th	< 2.5	< 1.4	< 0.8	0.9±0.3	< 0.4	< 0.33	< 0.43	< 0.26
^{235}U	^{235}U	< 1.6	< 0.8	< 1.0	< 3.1	< 0.6	< 0.69	< 0.82	< 0.3
	^{227}Ac/^{227}Th	< 4.3	-	-	< 6.1	< 1.9	< 1.8	< 2.0	< 1.2
	^{40}K	< 4.6	< 5.3	< 3.4	< 2.1	< 1.8	< 1.5	< 2.5	< 0.9
	^{138}La	< 0.6	< 0.7	< 0.7	< 0.5	< 0.3	< 0.29	< 0.31	< 0.20
	^{176}Lu	< 0.8	< 0.7	< 1.6	0.4±0.3	0.4±0.1	< 0.46	< 0.41	0.4±0.1
	^{134}Cs	< 0.24	< 0.4	< 0.23	< 0.24	< 0.09	< 0.09	-	< 0.06
	^{137}Cs	< 0.3	< 0.34	< 0.30	< 0.24	< 0.16	< 0.12	-	< 0.12

Table 3: *summary of measurement results for samples of Gd salts by company-B obtained by the specific-to-SkGd procedure. Units are mBq/Kg; limits are at 95% C.L. The 2017 measurements are shown in the three right-most columns.*

SuperKGd-lsc: the years to come

High purity Ge detectors are very powerful devices for obtaining a rather complete view of the radioactive contamination of a given material. In addition one could achieve a rather stringent upper limits in the case of high purity materials.

Table 5 shows the very restrictive requirements for a full physics program with SuperK-Gd. The lower ^{238}U chain and the whole ^{235}U are now routinely obtained within **SuperKGd-lsc.** Respecting the sensitivities to ^{238}U isotope and ^{232}Th upper and lower chain: even though they are excellent and give an almost definite assessment of the quality of the salt, an improvement of a factor of approximately 2 would be desirable.

This, which might be very difficult to achieve with Ge detectors, could be under reach by the LSC's new ICP-MS facility for the ^{238}U and ^{232}Th isotopes (because of the very long

Chaina	Main Sub-chain Isotope	GSF-1604-C-160303	GSF-1707-B-007	GSF-1710-C-170901	GSF-1710-C-170902	GSF-1710-C-170903
238U	^{238}U	< 20	< 10	< 9.7	< 12	< 11
	^{226}Ra	< 0.64	< 0.18	< 0.19	< 0.21	< 0.21
232Th	^{228}Ra	< 0.67	< 0.21	< 0.24	< 0.26	< 0.30
	^{228}Th	0.5 ± 0.2	< 0.26	< 0.28	< 0.31	< 0.30
235U	^{235}U	< 0.7	< 0.3	< 0.35	< 0.41	< 0.42
	^{227}Ac/^{227}Th	< 2.3	< 1.2	< 1.7	< 1.4	< 1.6
	^{40}K	< 1.6	< 0.9	< 0.8	< 1.0	< 0.7
	^{138}La	< 0.3	< 0.20	< 0.09	< 0.05	< 0.14
	^{176}Lu	< 0.4	0.8 ± 0.1	0.13± 0.03	0.11± 0.04	< 0.14
	^{134}Cs	< 0.1	< 0.06	< 0.08	< 0.06	< 0.07
	^{137}Cs	< 0.1	< 0.12	< 0.13	< 0.10	< 0.11

Table 4: *summary of measurement results of the 3 latest samples of Gd salts by company-C (see text for details). They are shown in the three right-most columns. The other two columns show the results for the best samples before the new ones, also from company-C (first column) and company-B (second). Units are mBq/Kg; limits are at 95% C.L.*

lifetimes). Needed sensitivities are at the 0.01 mBq/Kg level.

On the other hand, we have detected the presence of Cerium (Ce) in some of the delivered $Gd_2(SO_4)_3$ salts; remarkably the salt dissolved in the EGADS tank for more than 2.5 years shows approximately 45 ppm Ce content. Ce acts as a wavelength shifter -from

Radioactive chain	Part of the chain	SRN (mBq/kg)	Solar ν (mBq/kg)
^{238}U	^{238}U	< 5	-
	^{226}Ra	-	< 0.5
^{232}Th	^{228}Ra	-	< 0.05
	^{228}Th	-	< 0.05
^{235}U	^{235}U	-	< 3
	^{227}Ac / ^{227}Th	-	< 3

Table 5: *physics-based requirements for radioactive impurities in the Gd2(SO4)3 salt. Where no number is given (-), the corresponding requirement is less restrictive than that for the other physics analysis. SRN stands for "Supernova Relic Neutrino" and the relevant solar v are the low energy ones (below ~4 MeV kinetic energy).*

250 nm to the SK's sensitive 350 nm-, thus one immediate consequence is the change of the measured time-of-flight distributions. We estimate that a Ce content below 50 ppb is harmless for SuperK-Gd physic and that Ce can be easily measured with ICP-MS with a ~10 ppb accuracy.

The problem has been discussed with the LSC management that has considered very appropriate to provide as well for **SuperKGd-Isc** ICP-MS estimates of ^{238}U, ^{232}Th (~0.01 mBq/Kg resolutions) and Ce (~10 ppb resolution) of the samples that will be screened in the future.

Expectations for the medium and long-term futures

Figure 1 presents the scheme of a realistic approach to the whole production process by one of our partner companies

An example of production is 5 months' time for 2 tons (including the buying of material, modify drying facility, production). These 2 tons will be used for the production of the ultralow RI resin that will be used for further U and Ra removal at the pre-treatment (they will be screened as well by **SuperKGd-Isc**). The 10 tons for a first loading (at time T1) can be produce in ~8 months (buy material, modify production line, production). An overlap is expected in those 5 month and 8 month production periods.

The plan of the SuperK-Gd collaboration for purchasing the high purity $Gd_2(SO_4)_3$ is a) to order ~15 ton of Gd sulfate around Jun 2018, b) out of them, ~2 ton will be used for resin production and will be ready by winter of 2018 and c) the remaining ~13 t for SuperK-Gd will be ready by the beginning of Japanese FY2019.

Thus, we anticipate a full production type activity in RI screening from ~October 2018 to ~May 2019 (~ 15 tons) that will be hopefully followed by another year (maybe more) for the remaining 90 tons of full loading (at time T2), starting at ~June 2019.

We will be measuring at least one sample of every batch of the full production. Typically 1 production batch corresponds to approximately 500 kg. Therefore, for T1's 15 ton for resin production and loading, approximately 30 measurements have to be done, and 180 for the T2's remaining 90 ton.

Taking a typical measurement time of 20 days per sample, a full time Ge detector could cope with approximately 18 samples per year. Thus, for the ~9 month's duration of T1's mass production of ~30 samples, we would need a little bit more than 2 full time Ge detectors

Figure 1: *Realistic approach to full production schedule by one of the high purity Gd producers. FY stands for Japanese Fiscal Year.*

(30x20/270). For the ~13 months of T2's 90 tons (~180 samples) the estimate is ~9 full time Ge detectors (180x20/400).

Thus, the current ~1 Ge-detector/year "reserved" to SuperKGd-lsc plus the second detector approved by the LSC management for mass production periods, provide a rather significant contribution to the SuperK-Gd project. However more contributions will be helpful for the T1's 15 ton screening, and absolutely necessary for the final T2's 90 ton. This can only be achieved by incorporating outside contributions.

SuperKGd-lsc is leading a worldwide effort in such direction that includes the UK's Bulby Laboratory (via the Super-Kamiokande institute U. Sheffield) and the Kamioka Observatory itself.

10 GEODYN
GEOPHYSICS FROM UNDERGROUND

Geodyn is a geodynamical facility aimed to monitor seismic activity and tectonic deformation, using two continuous GPS stations at the surface and a broad-band seismometer, an accelerometer and two high-resolution laser strainmeters installed inside the tunnel. Three different teams are involved in the Geodyn management: ICTJA-CSIC, Barcelona, (Seismics), University of Barcelona (GNSS) and University of Salerno (Laser Interferometers).

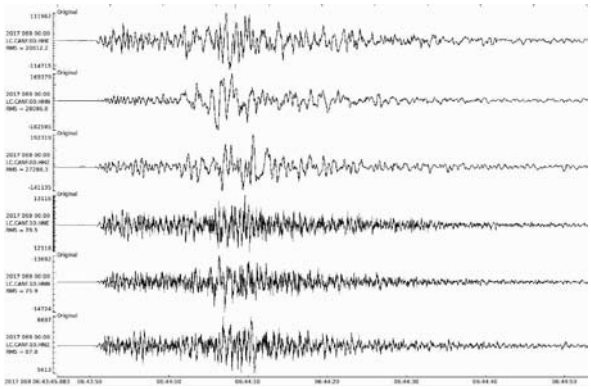

Figure 10.1: *The 10/3/17 event near Olave (Navarra) recorded by the six seismic components of the CANF station. Upper traces correspond to the broad-band seismometer (East-West, North-South and up-down) and the three other to the accelometric sensor (East-West, North-South and up-down).*

1 Seismic component

The Geodyn broad-band seismic sensor was sent to Nanometrics (Canada) for revision in September 2016. After some delays due to technical issues, the repair cost was approved March 15th and the instrument was repaired during summer and re-installed the 25th October 2017. The acquisition of seismic data during this time has been assured by a Trillium120 seismometer provided by ICTJA and recovered during the re-installation of the original instrumentation. All the seismic instruments have been working properly since then.

Up to 17 local events with magnitude over 3.0 and 140 events with magnitude over 2.0 have been reported by the IGN network in the vicinity of the LSC during 2017. The most significant local events have been the 10th March 2017 earthquake with moment magnitude 4.2 and epicenter near Olave (Navarra) (Figure 1) and the 26/4/2017 magnitude 3.9 event with epicenter near La Mongie, in the French side of the Pyrenees.

At regional scale, some of the events of the seismic crisis in Central Italy started in 2016 have been registered in early 2017, including four events with magnitudes ranging between 5.2 to 5.7 recorded the same day, the 18 th January 2017 (Figure 2).

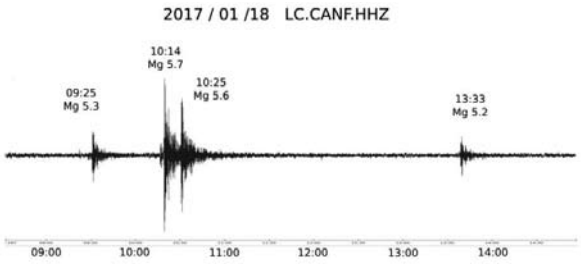

Figure 10.2: *Vertical component recording of the 4 events in Central Italy the 18/1/2017.*

Regarding teleseismic activity, up to 39 events with magnitude above 6.5 have been reported worldwide by the USGS catalog during 2017, 7 of them exceeding magnitude 7.0.

We can highlight the 8.1 Mw earthquake with epicenter near the Pacific coast of Mexico (8/9/17) and the 7.3 Mw earthquake near the Iran-Iraq border. Seismic waves generated by

those events have been clearly detected at CANF (Figures 3 and 4)

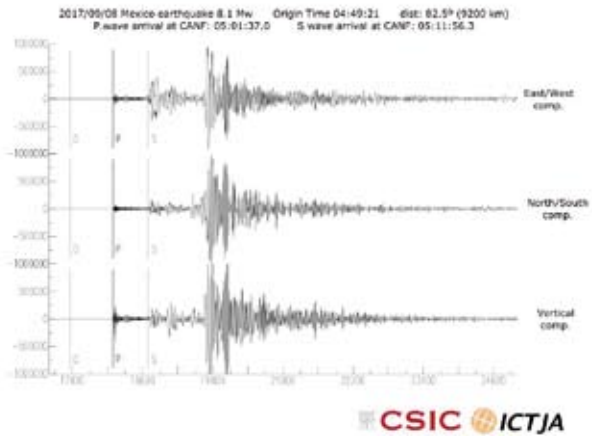

Figure 10.3: *The 8.1 Mw event with epicenter in the Pacific coast of Mexico recorded on the broad-band components of the CANF station. Time arrival for the P ans S waves are indicated.*

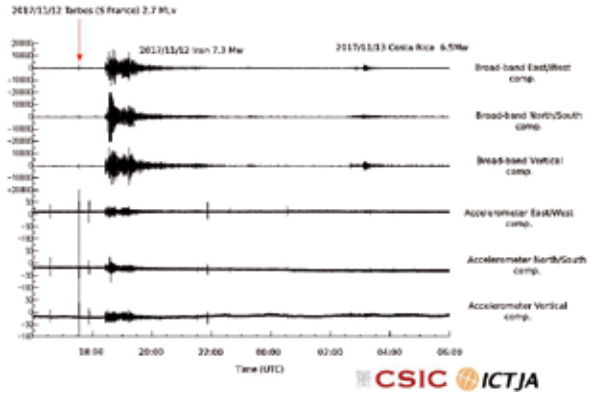

Figure 10.4: *The 7.3 Mw event with epicenter near the Iran/Iraq border, as recorded on the 6 components of the CANF station. The figure includes the record of the 13/11/17 event at Costa Rica as well as a local event near Tarbes (2.7 MLv).*

During 2017, the seismic sensors have continued to record also signals generated by different natural and anthropogenic sources. As an example, Figure 5 shows the vibration generated by the Ophelia storm passage as detected by different seismic stations in western Europe in October 2010.

2 Strain component

After some years of significant disturbances, the interferometers and the associated acquisition systems have been updated during 2017 and have then been running properly.

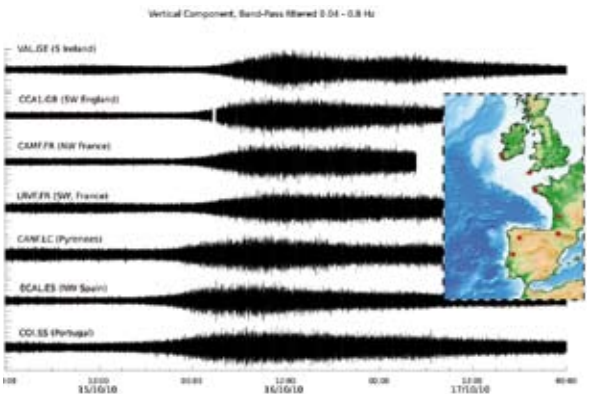

Figure 10.5: *The passage of the Ophelia storm as detected by permanent seismic stations in western Europe (red dots in the inset map). Data has been filtered between 0.04 and 0.8 Hz to retain the signal around the microseismic peak.*

Regarding the LAB780 interferometer, the equipment is running since December 2016 following the replacement of an old magneto-thermic circuit. The instrument has been running continuously since then, with a few short acquisition breaks due to our maintenance activity (slight re-alignment of the optics).

The laser source of the GAL16 interferometer has been sent back to the manufacturing Company (MicroGLacoste) by reason of malfunction in summer 2017, but is running again since September 2017. In the meantime, the LSC technicians have solved the problems generated by the presence from dust and mice: the protection box for the optics seems to work properly as well as the new electronics container (see Figure 6).

Figure 10.6: *New setup of the GAL16 main plinth*

The acquisition and pre-analysis codes have been heavily revised, resulting in faster conversion from photodiode light intensities

to strain, while keeping the same accuraccy. Sampling frequency of the photodiode light intensities has been increased from 600 Hz to 1000 Hz, hence allowing a better reconstruction of fast signals. Every few hours, strain files at 100 Hz, 1 Hz, and 0.1 Hz are produced and ready for visual pre-analysis.

A technical paper (Antonella Amoruso, Luca Crescentini, Alberto Bayo, Sergio Fernández Royo,Annamaria Luongo,"Two high-sensitivity laser strainmeters installed in the Canfranc Underground Laboratory (Spain): instrument features from 100 to 0.001 mHz") has been published on Pure and Applied Geophysics (doi: 10.1007/s00024-017-1553-7)

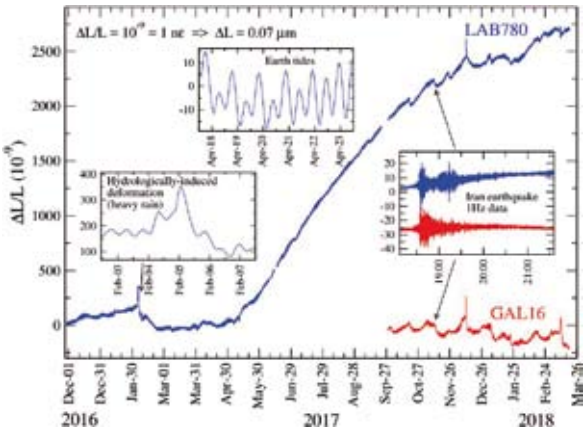

Figure 10.7: *Strain data recorded since December 2016. Insets show typical signals. Data have been decimated to 1 sample every 600 s (1 s for the Iran earthquake straingrams).*

Since May 2017 a quite unusual steep dilatation is being recorded by the LAB780 interferometer (Figure 7). By the end of the year this dilatation shows a somewhat slower rate. This pace change seems to exclude a hydrological origin related to the scarce precipitation during 2017, although at this point, the origin of this feature remains unclear.

3 GNSS component

Following the installation of large capacity USB memory devices during the second half of 2016, the two GNSS stations have been working properly during the first months of 2017.

Later on, CAND station, located at Candanchú, has been un-operational from May 15th, 2017 due to the modem or external memory related problems. Fortunately, GNSS receiver itself as been working properly and the station has been storing the acquired data in its internal memory. These problems were solved in November 15th, 2017 by changing the memory card. Since the 4-char CAND was in conflict with the existing CGPS station used by the global community, we have opted to change the 4-char abbreviation from CAND to CNDC.

RAPI station, located at Fuerte de Rapitán near Jaca, has been operated with some interruptions, in particular during the second half of the year.

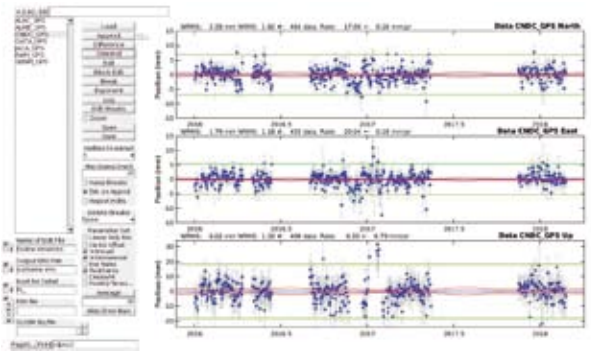

Figure 10.8: *Screen shot of the detrended time-series of the CNDC station from 1/2/2016 to 1/3/2018. Some gaps in the data are due to the missing files, and others are due to filtering of the outliers.*

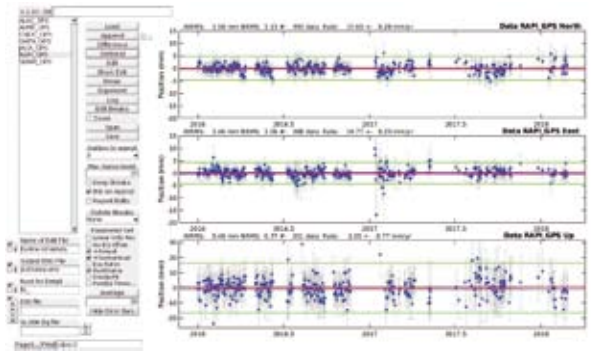

Figure 10.9: *Screen shot of the detrended time-series of the RAPI station from 1/2/2016 to 1/3/2018. Some gaps in the data are due to the missing files, and others are due to filtering of the outliers.*

Data from both stations has been downloaded by the Univ of Barcelona team on a weekly basis and the recorded data have been processed to obtain the daily positions for both sites. Figures 8 and 9 present the results of the preliminary analysis of the data from the CNDC and RAPU CGPS stations using the GAMIT/GLOBK software by MIT. The velocity rates that appear on top of the time-series are in ITRF2008 reference frame and need to be transformed to Eurasia fixed reference frame to ease the interpretation of the results.

11 GOLLUM
LIFE IN EXTREME ENVIRONMENTS

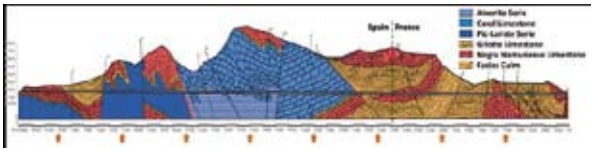

Fig. 11.1 Morphology of rocks around the Canfranc railway tunnel.

The Somport tunnel crosses different sedimentary rocks built by accumulation of sediments in the Mesozoic and Cenozoic ages (see Fig. 11.1). Its length, depth and diverse ecology make it a perfect site for extremophile ecology studies. In extreme environments, bacteria –and archaea- tend to be the main living organisms. Subterranean microorganisms have been described to sum detail, but almost all reports refer to samples taken centimetres to few meters below the surface. In fact, many of those have a photoautotrophic metabolism. By contrast, the literature describing microorganism inhabiting the very inside of rocks are scarce. The few reports, analysing the microbial diversity of rock inhabitants evidence, a rather high diversity of microbial taxa and metabolism pathways, including bacterial groups such as green non-sulfur, sulfur or iron reducing, and also methan producers, amongst others.

GOLLUM goal is the identification and characterization of the microbial communities living in a range of different rocks throughout the length of the Somport tunnel, from the surface to the maximum depth. This will be accomplished through 16S amplicon and shotgun high throughput sequencing of the combined genomes in a given sample (metagenomics). Taken together, these procedures will allow determining with high precision the microbial composition of the Somport tunnel at different depths and on different mineral substrates. Sampling different depths and rocks will be achieved by collecting one-meter length cylinders of rock drilled along the tunnel, minimizing external contamination. Improved protocols are needed for desoxyribonucleic acid (DNA) extraction of the scarce genetic material sampled. Recent progress in high throughput next generation sequencing is leading to the discovery of numerous new species of bacteria and archaea, non-cultured by standard methods.

GOLLUM collaboration drilled 14 cores in locations placed along the train tunnel in May 2016, in sterile conditions required for DNA extraction and genomic studies of low DNA samples (see Fig. 12.2). We have developed techniques to obtain rock powder with grain sizes in the range 10 -100 microns and extraction protocols of low DNA content in carbonated samples (with sensitivity of one in 10 billion in DNA grams per gram). Genomic sequencing was performed in Sistemas Genomicos laboratories. The archaea content in one of our samples is shown in the figure. We show the 4% of the classified DNA reads, which correspond to archaea. Most of the archaea species have be identified with taxa discovered in submarine soils.

Chemical studies of the sampled rocks using, among other techniques, X-ray fluorescence, show a correlation of the DNA content in archaea with the presence of some metals, particularly Molybdenum (Mo), a metal identified in proteins associate to methanogenesis. The figure shown below is the X-ray fluorescence spectrum of samples with positive (negative) DNA presence in green (red). When comparing the spectra, we can see a significant variability in metal abundances and particularly the presence/absence of the Mo peak. The DNA reads from whole genome sequencing provide more information that the taxonomic

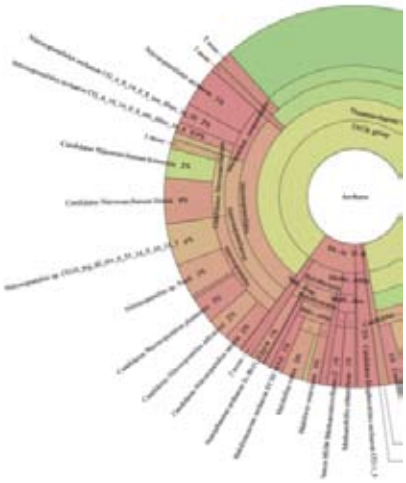

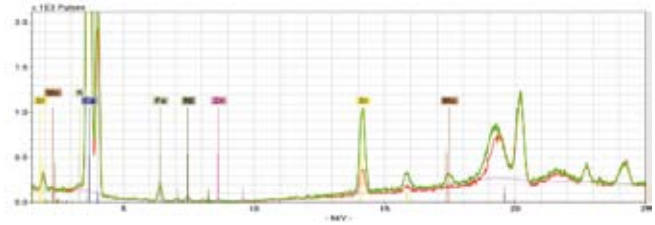

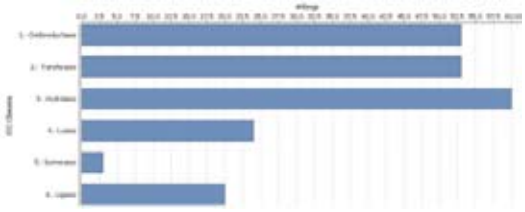

characterization. Gollum is exploiting the potential of the data to characterize the variations of enzyme distributions (shown in the figure) as a function of the sample, which opens the door to correlate metabolic activity with metal content in rocks.

Our project is shedding light on a barely explored extreme environment, characterized by poor nutrients, diverse physicochemical substrates, moderate radiation levels (in some cases), and very narrow temperature fluctuations. The presence of native DNA, a first success of the experiment, opens many questions, starting by asking whether the biological material corresponds to relic DNA or living cells. The originality of the Somport tunnel as a "highway to depths", its geological diversity and the potency of the methods we plan to use may yield an unprecedented complex matrix of data on the microbial biocenoses of subterranean habitats, with both fundamental (origin of life, astrobiology) and applied (bioprospection, discovery of new species) important consequences.

12 TREX-DM
LIGHT DARK MATTER WITH A GASEOUS TARGET

http://gifna.unizar.es/trex/

TREX-DM aims at detecting Dark Matter particles (WIMPs) of particularly low masses (below ~10 GeV). The mainstream search strategies so far have been targeting a somewhat heavier WIMP mass (around 100 GeV), as it is the natural expectation from the "WIMP miracle" argument (that rather generically links the mass, annihilation cross-section and relic density of WIMPs). However, despite many years of efforts, and impressive advances in detectors' sensitivity, such "standard" WIMPs have not yet been found. In addition, Supersymmetry, the most appealing (hypothetical) theoretical framework to host these particles has not been experimentally shown at the Large Hadron Collider of CERN. Due to this, an increasing effort is now being devoted to consider alternative, a priori less standard, hypothesis.

The possibility that WIMPs are of masses below 10 GeV is still possible in particular supersymmetric models or, alternatively, in other theoretical frameworks not necessarily linked to supersymmetry. If that were the case, dark matter could very well be made of WIMPs but not have shown in current mainstream experiments, no matter how sensitive. This is because nuclear recoils produced by such low-mass WIMPs have energies that typically lay below the experimental energy threshold. Dark matter detectors with nuclear-electron recoil discrimination are effectively limited in threshold by the discrimination capability. Sensitivity to low mass WIMPs requires a different approach and different challenges: the focus is set primarily on low threshold, and secondarily on low background. Nuclear-electron recoil discrimination is not available at the energies of interest (1 keV and below), and background sources in these energies are still poorly studied. Due to the relatively larger background levels, detector exposure is of less importance, and light and small detectors can still have competitive sensitivity.

TREX-DM is addressing these challenges with a detection approach that is unique in its kind in the field. TREX-DM is a high-pressure charge-readout gaseous time projection chamber (TPC) with a relatively light atomic species as target medium (Argon- or Neon-based mixtures are considered). The signal amplification inherent to gas detectors, combined with the light target nuclei, allows having very low energy thresholds for a dark matter detector. The current TREX-DM detector aims at energy thresholds of 0.1-0.4 keV electron-equivalent, with prospects for improvement in the future.

The detector is built with the highest radiopurity standards, and is surrounded by a massive lead-and-copper castle to shield it from external radiation. Figure 12.1 shows a design of the full setup, as it will be in its final configuration at the LSC. The body of the vessel is built of high purity copper and all components made from radiopure materials, selected after an exhaustive screening campaign. The sensitive volume of the detector is composed by two side-by-side TPC sharing the high voltage cathode in the middle. Figure 12.2 shows the sketch of the detector

vessel and the inside TPC layout. The charge amplification and sensing is achieved with 2 Micromegas readout planes, placed at each of the TPC ends. A picture of one of the Micromegas planes is shown in Figure 12.3, installed on top of one of the detector endcaps during its installation in the laboratory. The Micromegas are built with the "microbulk" technique, which features the highest radiopurity standards among sensor planes, as they are made exclusively out of copper and kapton. The readouts are finely pixelated and read out by low-noise high density TPC electronics, which are placed outside the shielding. The pixelization allows for higher electronic signal-to-noise ratio, and therefore lower threshold, as well as for event localization and topological information. The approximately 1000 signal channels are taken out of the detector vessel and shield by ultraclean flat cables and solder-less high-density contact connectors.

The microbulk technology and the technical solutions to implement a highly radiopure Micromegas TPC are the outcome of the ERC-funded TREX project at the University of Zaragoza.

During 2017 the detector has been prepared for underground operation and commissioned on surface. In parallel, the experiment site underground at LSC has been prepared. At the beginning of 2018 the detector has finally been transported to LSC. Figure 12.4 shows

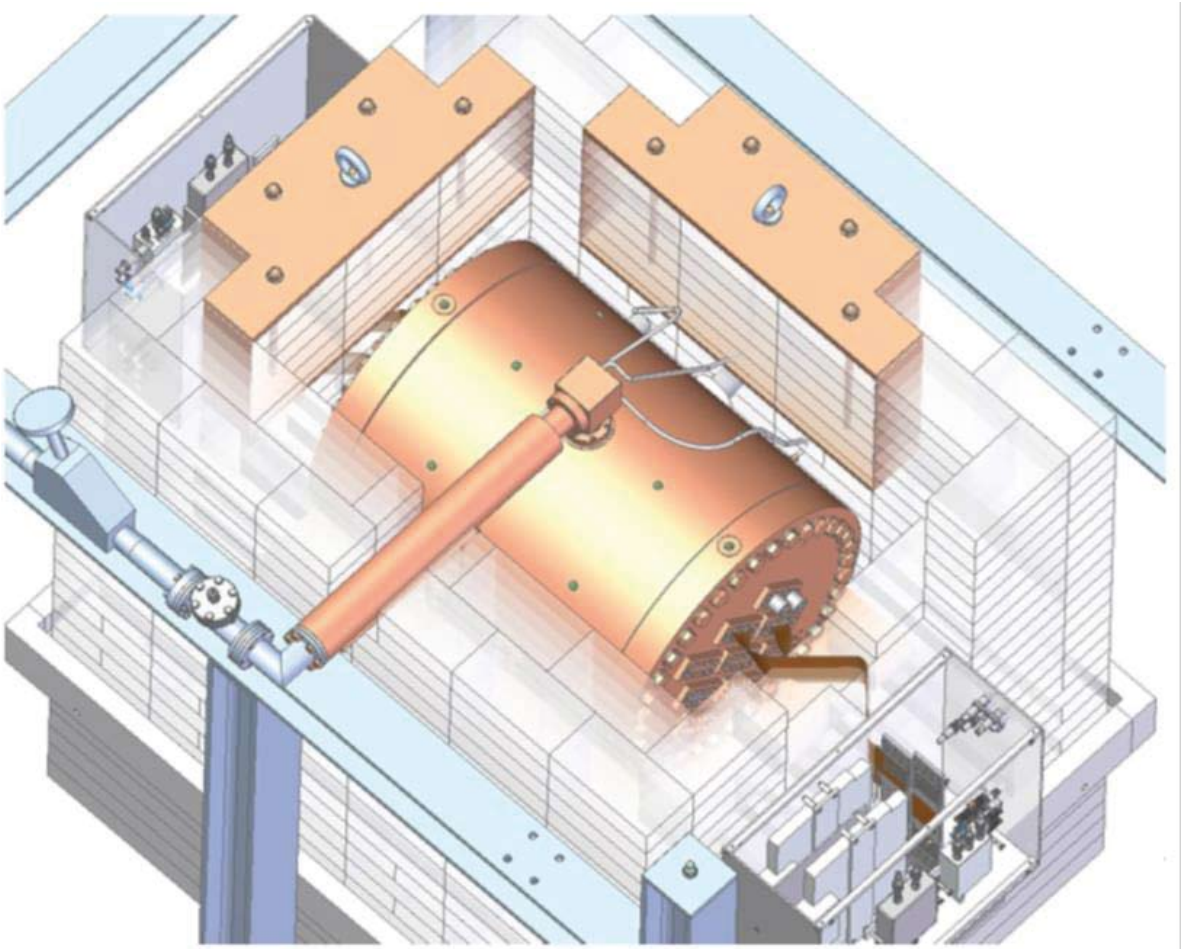

F gure 12.1.- *Drawing of the TREX-DM experiment, showing the detector surrounded by part of the shielding*

the detector being reassembled at the LSC clean room, before being moved to the final site at the Hall A of LSC.

In the coming months TREX-DM is expected to start physics data taking. If the experimental parameters anticipated in the design phase are achieved, TREX-DM can reach competitive sensitivity and probe unexplored parameter space in the low mass range. In any case, TREX-DM will be an invaluable tool to study background sources in the energy range around and below the keV, a knowledge that is critical in the novel experimental frontier that is emerging at low WIMP masses.

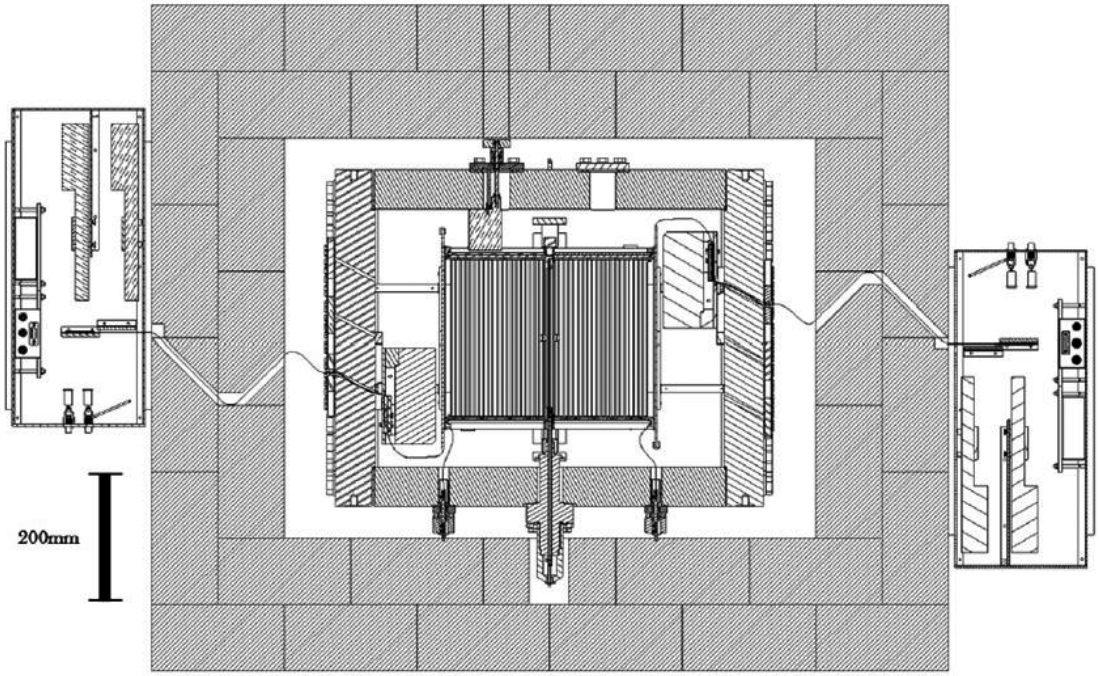

Figure 12.2.- *Layout of the experiment showing the TPC, copper vessel, lead shielding adn the DAQ electronics at the two sides*

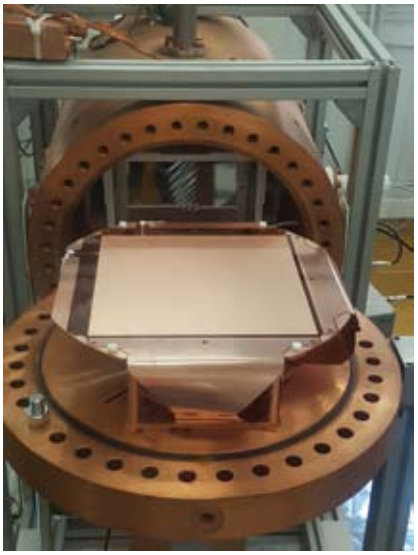

Figure 12.3.- *Picture of one of the Micromegas readout planes, installed on one of the vessel endcaps of the TREX-DM detector*

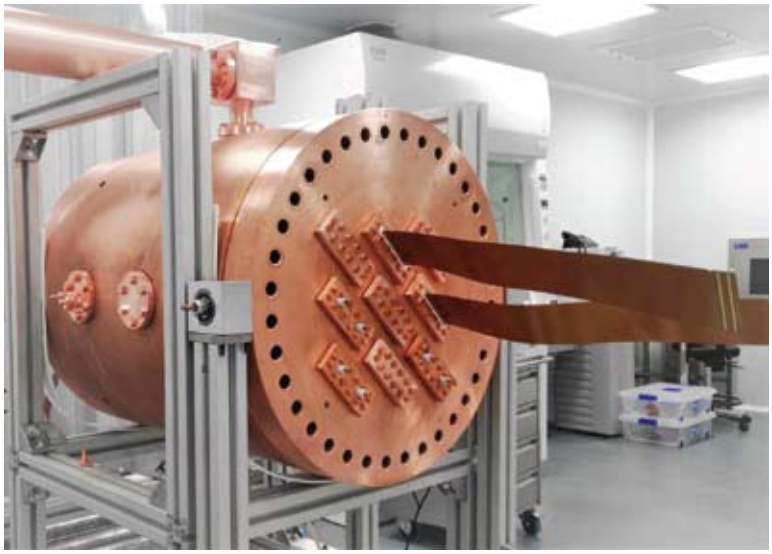

Figure 12.4.- *Picture of the TREX-DM detector being reassembled in the clean room of LSC*

13 ETSEC
EINSTEIN TELESCOPE SEISMIC EXPLORER IN CANFRANC

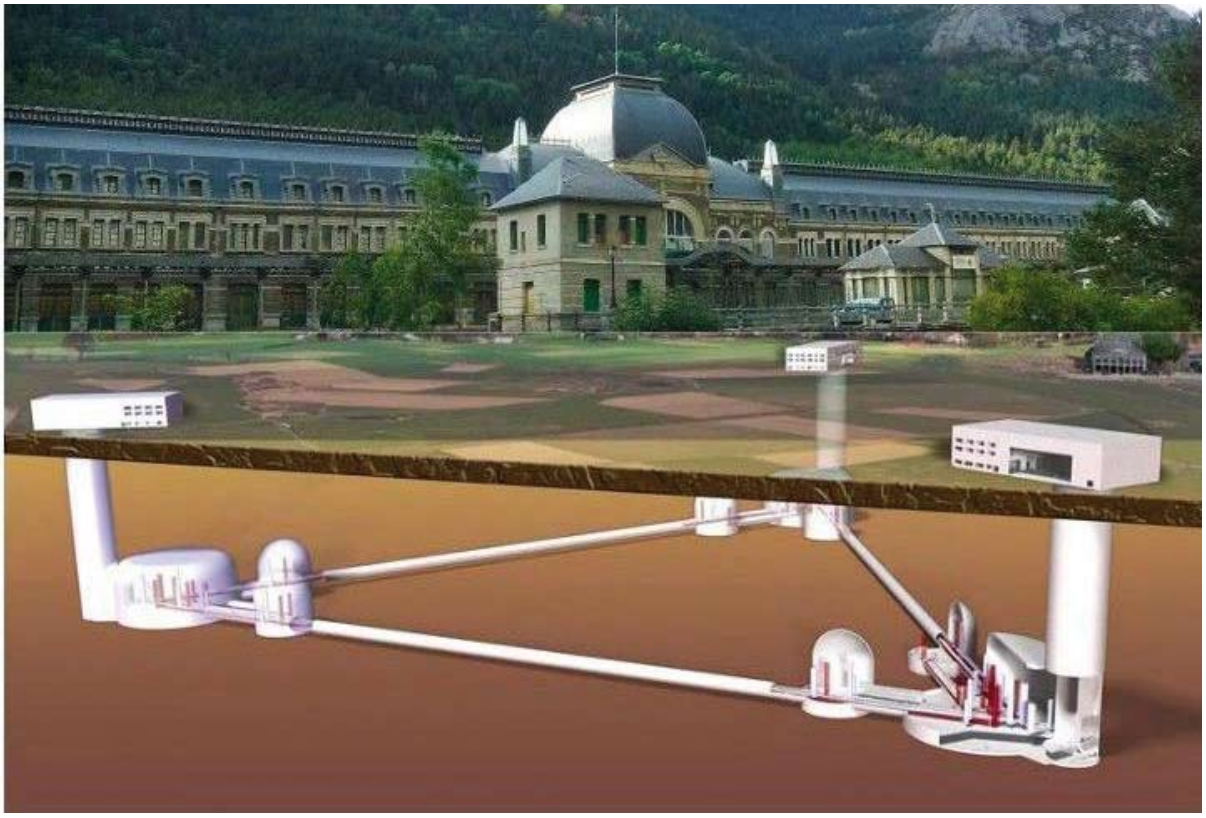

Einstein Telescope is a project to build an extremely sensitive next generation gravitational wave detector. The ETSEC project proposes to characterize the seismic environment at Canfranc with the aim of considering it as a candidate site for construction of the Einstein Telescope.

The long search for gravitational waves was awarded with success in 2016 with the first detection of a coalescence of two black holes by LIGO (Abbott et al 2016). This discovery marked the onset of the beginning of the new branch of science - the gravitational wave astronomy. The LIGO detector started taking data again in 2017 and it was joined by VIRGO. The joint observations lead to discovery of several new binary black hole systems and a binary neutron star merger GW170817 accompanied by a gamma ray burst. This discovery marked the onset of the multimessenger astronomy.

The beginning of the gravitational wave astronomy has raised several questions about the future developments. The current instruments should be considered as pathfinders that will lead the way for the future instruments. There are two paths to develop gravitational wave astronomy. The first is to search for sources in other frequency ranges. The LISA experiment will look for gravitational waves in the low frequency regime. The second is to construct telescopes that will be able to probe the Universe with much higher sensitivity in the

same, or slightly enhanced frequency band. The Einstein Telescope (Punturo 2010a) project aims to reach this goal.

The Einstein Telescope project aims at a constructing an underground array of three interferometers with the 10 km arm length. The main reason for the underground construction is to allow a better sensitivity at low frequencies, below 10Hz. In this band the sensitivity is limited by the seismic noise but at the expected sensitivity of the Einstein Telescope the gravity gradient or Newtonian noise will also play a role. The seismic noise is known to decrease when going underground. The preliminary measurements of the seismic noise level at Canfranc were performed previously (Beker 2015), and it has been shown to be one of the seismically most quiet sites under consideration. However, this is based on a very short stretch of data, taken at a single location.

The site requirements for the Einstein have not been formalized yet. Nevertheless we are looking for sites with a very small seismic noise level in the band from 0.1 to 20Hz. Moreover, the noise at the site should be stable with little or no daily or seasonal variation. Additionally the site should be accessible and should have some infrastructure as well as science support available. As such, the Canfranc area is a very good potential candidate for construction of the Einstein Telescope. However, the noise from the traffic at the road tunnel needs to be characterized. Additionally, the Canfranc railway tunnel with the escape connecting tunnels to the road tunnel forms a very good environment to study seismic wave propagation and a laboratory for Newtonian noise modeling.

We are performing the seismic noise measurements at Canfranc with the aim of characterizing the area as a potential site for the Einstein Telescope. In particular we want to characterize:

- The seismic noise level
- The seismic noise variation as a function of the time of the day
- The seismic noise seasonal variation
- Gather the data for newtonian noise modeling

To this end we have installed six time synchronized seismic sensors. We foresee the duration of the project to be three years. While the seismic noise can be measured in much shorter time we would like to be able to measure the seasonal variation of the noise, and hence such an extended timeline. The measurements are done with the custom-made seismic sensors. The single sensor uses three single axis seismometers, one for vertical and two for horizontal measurements. The three sensors are mounted in the metal housing, shown in Figure 13.1.

Fig.13.1: *The seismic sensor mounted on a steel plate. The top two connectors are used for data communication, while the bottom one is used to provide power..*

The sensors are connected in series in such a way that the seismic noise is measured by all of the sensors in the same time. In such a configuration the connecting cable between the sensors are used to transmit data and

for synchronizations of all sensors. The data from the sensors are recorded by the data acquisition unit (DAU) placed in Lab 2500. Each sensor uses communication cable which is incoming from previous sensor or DAU and outcoming for next sensor. The third connector provides power supply 230 V. An example of connection sensors is shown in Figure 2.

During 2017, the works at Canfranc covered mainly preparatory activities. These included:

1. Selection of the locations for the sensors
2. Obtaining the necessary permits for the installation
3. Construction of the concrete stands for the sensors
4. Preparation of the equipment in Warsaw
5. Shipment of the equipment to Canfranc
6. installation of the sensors and initial data taking.

Currently the ETSEC team is performing the data analysis and we are acquiring more data.

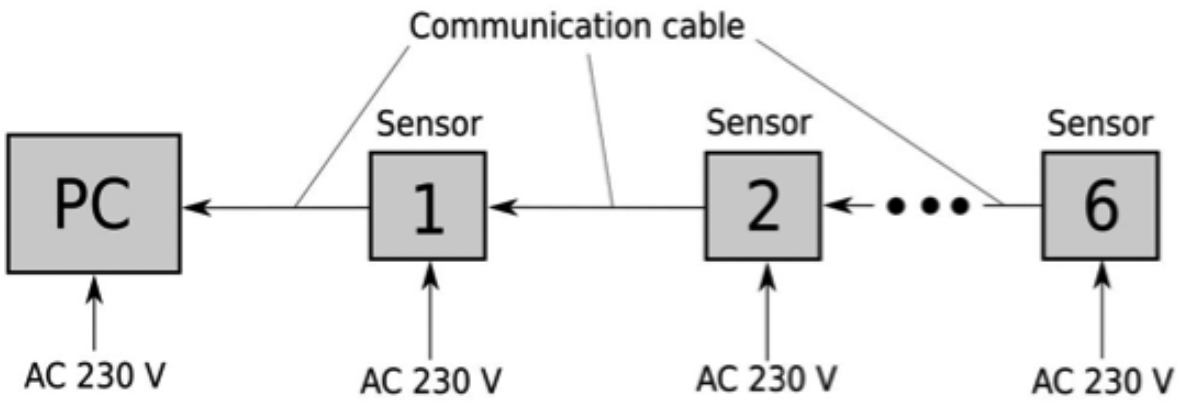

Fig.2: *Connection diagram of six seismic sensors.*

PUBLICATIONS IN REFEREED JOURNALS

Review of technical features in underground laboratories Ultra-low background and environmental measurements at Laboratorio Subterráneo de Canfranc (LSC) S. Borjabad et al., ARI journal volumen 126 (August 2017, ISSN 0969-8043)

Applied Radiation and Isotopes 126 (2017) 127-126
I. Bandac et al., El Sevier
http://dx.doi.org/10.1016/j.apradiso.2016.12.038

Characterization of a CLYC detector for underground experiments
A. Ianni, I. Bandac et al., arXv:1710,02420vl, 6 Oct 2017
http://arxiv.org/abs/1710.02420v1

The ANAIS-112 experiment at the Canfranc Underground Laboratory, J. Amaré et al.
Contributed to the TAUP2017 Conference, Sudbury, Canada, July 2017.
https://arxiv.org/abs/1710.03837

Annual modulation of dark matter: the ANAIS-112 case, I. Coarasa et al.
http://arxiv.org/abs/1704.06861

Light yield determination in large sodium iodide detectors applied in the search for dark matter, M.A. Oliván et al.
Astroparticle Physics 93 (2017) 86-95
https://doi.org/10.1016/j.astropartphys.2017.06.005
http://arxiv.org/abs/1703.01262

The ANAIS Dark Matter Project: Status and Prospects, J. Amaré et al.
Proceedings of the 14th Marcel Grossmann Meeting, July 2015, Rome, Italy.
Published by World Scientific, Dec 2017. Edited by M. Bianchi, R. Jantzen & R. Ruffini. ISBN: 978-981-3226-59-3. pg 2414 – 2419.
http://arxiv.org/abs/1601.01184
http://www.worldscientific.com/doi/pdf/10.1142/9789813226609_0283

The NEXT Collaboration (C.A.O. Henriques et al.), Secondary scintillation yield of xenon with sub-percent levels of CO 2 additive for rare-event detection, Phys.Lett. B773 (2017) 663-671.

The NEXT Collaboration (C. Azevedo et al.), Microscopic simulation of xenon-based optical TPCs in the presence of molecular additive, Nucl.Instrum.Meth. A877 (2018) 157-172.

The NEXT Collaboration (S. Cebrián et al.), Radiopurity assessment of the energy readout for the NEXT double beta decay experiment, JINST 12 (2017) no.08, T08003.

The NEXT Collaboration (A. Simón et al.), Application and performance of an ML-EM algorithm in NEXT, JINST 12 (2017) P08009.

The NEXT Collaboration (J. Renner et al.), Background rejection in NEXT using deep neural networks, JINST 12 (2017) no.01, T01004.

L. Crescentini et al, Two High-Sensitivity Laser Strainmeters Installed in the Canfranc Underground Laboratory

ArDM Collaboration, Calvo, J., et al. "Backgrounds and pulse shape discrimination in the ArDM liquid argon TPC", e-Print: arXiv:1712.01932 (2017).

ArDM Collaboration, J. Calvo et al., "Commissioning of the ArDM experiment at the Canfranc underground laboratory: first steps towards a tonne-scale liquid argon time projection chamber for Dark Matter searches," Journal of Cosmology and Astroparticle Physics 2017 (2017) 003, e-Print: arXiv:1612.06375 [physics.ins-det].

The ArDM Liquid Argon Time Projection Chamber at the Canfranc Underground Laboratory: a ton-scale detector for Dark Matter Searches
JCAP03(2017)003 doi:10.1088/1475-7516/2017/03/003

Backgrounds and pulse shape discrimination in the ArDM liquid argon TPC
arXiv:1712.01932 [physics.ins-det] submitted to JCAP

Martí JM, Martínez-Martínez D, Rubio T, Gracia C, Peña M, Latorre A, Moya A, P Garay C. 2017. 16.
Health and disease imprinted in the time variability of the human microbiome. mSystems 2:e00144-16 https://doi.org/10.1128/mSystems.00144-16

TREX-DM: a low-background Micromegas-based TPC for low-mass WIMP detection
I Garcia Irastorza et al., Eur. Phys. J. C (2016) 76: 529

The BiPo-3 detector. P. Loaiza et al. [SuperNEMO Collaboration]. Appl. Radiat. Isot. 123, 54 (2017).

The BiPo-3 detector for the measurement of ultra low natural radioactivites of thin materials. A. S. Barabash et al. [SuperNemo Collaboration]. JINST 12 P06002 (2017).

Thesis

M. Nebot Guinot, Calibration and background model of the NEW detector at the LSC. 27 Septiembre 2017

Javier Pérez, Radioactive Contamination in Neutrino Experimental Physics: the Cases of NEXT and Super-Kamiokande Experiments, Septiembre 2017.

A. Simón Estevez, Event reconstruction in NEXT using a ML-EM algorithm. 15 de Septiembre 2017

J. Rodriguez, Study and design of the front-end and readout electronics for the tracking plane in the NEXT experiment. 26 Julio 2017

During 2017, 15 presentations to International Scientific Conferences have been made by users of the LSC.

GOVERNING BODIES

Governing Council

Juan María Vázquez Rojas, Secretario General de Ciencia e Innovación, Ministerio de Economía y Competitividad

Maite Gálvez Jaqués, Directora General Técnica del Departamento de Innovación, Investigación y Universidad, Gobierno de Aragón

Luis Miguel García Vinuesa, Vicerrector de Política Científica, Universidad de Zaragoza

Ángela Fernández Curto, Subdirectora General Adjunta de Grandes Instalaciones Científico Tecnológicas, Ministerio de Economía y Competitividad

Marina Villegas, Directora Agencia Estatal de Investigación, Ministerio de Economía y Competitividad

Fernando Beltrán Blázquez, Secretaría General Técnica del Departamento de Innovación, Investigación y Universidad, Gobierno de Aragón

Pilar Zaragoza Fernández, Vicerrectora de Transferencia e Innovación Tecnológica, Universidad de Zaragoza

Executive Committee

Ángela Fernández Curto, Subdirectora General Adjunta de Grandes Instalaciones Científico Tecnológicas, Ministerio de Economía y Competitividad

Francisco Herrada Martín, Jefe del Área de la Subdirección General Adjunta de Planificación de Infraestructuras Científicas y Tecnológicas, Ministerio de Economía y Competitividad

Fernando Beltrán Blázquez, Secretaría General Técnica del Departamento de Innovación, Investigación y Universidad, Gobierno de Aragón

Maite Gálvez Jaqués, Directora General Técnica del Departamento de Innovación, Investigación y Universidad, Gobierno de Aragón

Luis Miguel García Vinuesa, Vicerrector de Política Científica, Universidad de Zaragoza

Eduardo García Abancéns, Director del Área Política Científica del Vicerrectorado de Investigación, Desarrollo e Innovación, Universidad de Zaragoza

ADVISORY COMMITTEES

International Advisory Committee

David Sinclair (Presidente) - Carleton University (Canada)

Frank T. Avignone - University of South Carolina (USA)

Antonio Bueno Villar- Universidad de Granada, Granada (Spain)

Cristiano Galbiati - Princeton University, New Jersey (USA)

Andrea Giuliani - CSNSM, Orsay Campus (France)

Berta Rubio Barroso - CSIC, Instituto de Física Crepuscular, Valencia (Spain)

Mark Chen - Queen's University, Ontario (Canada)

Eligio Lisi - INFN, Bari (Italy)

Paola Tropea - CERN, Geneva (Switzerland)

ACKNOWLEDGMENTS

LSC is grateful to the Spanish Ministerio de Economía Industria y Competitividad, the Gobierno de Aragón and the Universidad de Zaragoza for providing the financial support from which to pursue its mission of fundamental research and outreach. LSC is also very grateful to the Major of Canfranc and to the Control System of the Somport Tunnel for the positive collaboration.

LSC

Laboratorio Subterráneo de Canfranc